

Genomic analysis of Ostreococcus tauri-infecting viruses reveals a hypervariable region associated with host–virus interactions

Julie Thomy, Julien Henri, David Demory, Frederic Sanchez, Marie-Line Escande, Gilles Mirambeau, Nigel Grimsley, Sheree Yau

▶ **To cite this version:**

Julie Thomy, Julien Henri, David Demory, Frederic Sanchez, Marie-Line Escande, et al.. Genomic analysis of Ostreococcus tauri-infecting viruses reveals a hypervariable region associated with host–virus interactions. Virus Evolution, 2026, ⟨10.1093/ve/veaf096⟩. ⟨hal-05370419v2⟩

HAL Id: hal-05370419

https://hal.sorbonne-universite.fr/hal-05370419v2

Submitted on 18 Feb 2026

HAL is a multi-disciplinary open access archive for the deposit and dissemination of scientific research documents, whether they are published or not. The documents may come from teaching and research institutions in France or abroad, or from public or private research centers.

L'archive ouverte pluridisciplinaire **HAL**, est destinée au dépôt et à la diffusion de documents scientifiques de niveau recherche, publiés ou non, émanant des établissements d'enseignement et de recherche français ou étrangers, des laboratoires publics ou privés.



Distributed under a Creative Commons CC BY 4.0 - Attribution - International License

VIRUS EVOLUTION

Virus Evolution, 2026, **12(1)**, veaf096
DOI: https://doi.org/10.1093/ve/veaf096
Advance Access Publication 11 February 2026
Research Article

Genomic analysis of *Ostreococcus tauri*-infecting viruses reveals a hypervariable region associated with host–virus interactions

Julie Thomy [1,2,*], Julien Henri [3], David Demory [4], Frederic Sanchez[1], Marie-Line Escande[1], Gilles Mirambeau[4], Nigel Grimsley[4], Sheree Yau [4,*]

[1]Integrative Biology of Marine Organisms (BIOM), UMR7232, Sorbonne University, CNRS, Oceanographic Observatory of Banyuls-sur-Mer, 20 Avenue Pierre Fabre, F-66650 Banyuls-sur-Mer, France
[2]Daniel K. Inouye Center for Microbial Oceanography: Research and Education, School of Ocean and Earth Science and Technology (SOEST), University of Hawai'i at Mānoa, 1950 East-West Road, Honolulu, HI 96822, United States
[3]The Laboratory of Computational and Quantitative Biology (LCQB), Institute of Biology Paris-Seine, Sorbonne University, CNRS, 4 Place Jussieu, F-75005 Paris, France
[4]Laboratory of Biodiversity and Microbial Biotechnology (LBBM), Sorbonne University, CNRS, Oceanographic Observatory of Banyuls-sur-Mer, 20 Av. Pierre Fabre, F-66650 Banyuls-sur-Mer, France

*Corresponding authors. Julie Thomy, Integrative Biology of Marine Organisms (BIOM), UMR7232, Sorbonne University, CNRS, Oceanographic Observatory of Banyuls-sur-Mer, Banyuls-sur-Mer, France. Daniel K. Inouye Center for Microbial Oceanography: Research and Education, School of Ocean and Earth Science and Technology (SOEST), University of Hawai'i at Mānoa, 1950 East-West Road, Honolulu, HI 96822, United States. E-mail: thomy@hawaii.edu; Sheree Yau, Laboratory of Biodiversity and Microbial Biotechnology (LBBM), Sorbonne University, CNRS, Oceanographic Observatory of Banyuls-sur-Mer, 20 Avenue Pierre Fabre, F-66650 Banyuls-sur-Mer, France. E-mail: sheree.yau@obs-banyuls.fr.

Abstract

While the genus *Prasinovirus*, known to infect prasinophyte green algae (class Mamiellophyceae), is abundant in the oceans, the genetic mechanisms governing the ecology and (co)evolution of these viruses remain poorly understood. In this study, we sequenced the complete genomes of eighteen viruses infecting the cosmopolitan unicellular green alga *Ostreococcus tauri* (OtVs) and one specific to *Micromonas commoda* (McV-20 T). Of these viruses, 12 were previously isolated from the coastal Mediterranean Sea and seven were newly isolated from two different geographical locations (i.e. the South Pacific Ocean and the North Sea). Phylogenetic analysis classified these viruses as new members of the *Prasinovirus* genus and defined three distinct OtV clades: designated OtV-type 1, OtV-type 2a, and OtV-type 2b. The OtV-type 1 includes three new viruses isolated from the Pacific Ocean and the previously sequenced genome OtV6. The OtV-type 1 form a large cluster within the *Micromonas*-infecting virus clade, sharing five unique homologous genes with all *Micromonas* viruses. In addition, genetic features of OtV-type 1, including a higher number of CDSs (~260) and lower Guanine-Cytosine content (GC) content (~41%), were more closely allied to *Micromonas* viruses than to those of OtVs, suggesting an alternative host or a recent host switch from *Micromonas* to *O. tauri*. By analysing the OtV genomes, we found a faster-evolving central hypervariable region (HVR), where the OtV-type 2b displayed the largest region, i.e. three times longer than other OtVs. This region encodes genes mainly associated with host cell recognition and attachment and under strong selective pressure (positive and negative). Notably, most viruses associated with OtV-type 2b showed the broadest host range. Infection dynamics between the hosts and the viruses appeared highly specific to host–virus pairs, suggesting complex interactions in the *Ostreococcus*-prasinovirus system. Finally, by observing viral lysates with electron microscopy, we observed novel morphologies never described for these viruses. Overall, this study provides new insights into the genetic diversity of prasinoviruses and describes for the first time a viral plasticity that might be strongly shaped by antagonistic coevolution with their hosts.

Keywords: *Nucleocytoviricota* Mamiellophyceae; phytoplankton; *Ostreococcus tauri* viruses; *Prasinovirus ostreotauri* host specificity; coevolution

Introduction

Viruses are described as the most common and diverse parasites in the oceans (Suttle 2005, 2007). Through cell lysis, marine viruses play a major role in marine ecosystems and microbial food webs by facilitating recycling of organic matter and nutrients (Fuhrman 1999, Wilhelm and Suttle 1999, Guidi et al. 2016, Middelboe and Brussaard 2017, Mayers et al. 2023). Beyond mortality, they also strongly shape the evolution of their host (Thingstad 2000, Weinbauer 2004, Friman and Buckling 2013), by driving host microdiversity (i.e. intragenomic diversity) (Fuhrman and Campbell 1998, Moore et al. 1998) through genetic mechanisms, such as mutations, horizontal gene transfers, and viral resistance (Avrani et al. 2011, Marston et al. 2012). The evolution of viral genomes is also strongly shaped by their host (Retel et al. 2019). Viruses and their hosts often undergo antagonistic coevolution, marked by reciprocal genetic exchanges over time (Martiny et al. 2014). These dynamics involve ongoing evolution, where the host evolves mechanisms to resist the antagonist, and the antagonist evolves counter-strategies to overcome the defences of the host (Van Valen 1974). In this way, the coevolutionary

© The Author(s) 2026. Published by Oxford University Press.
This is an Open Access article distributed under the terms of the Creative Commons Attribution License (https://creativecommons.org/licenses/by/4.0/), which permits unrestricted reuse, distribution, and reproduction in any medium, provided the original work is properly cited.

Downloaded from https://academic.oup.com/ve/article/12/1/veaf096/8472608 by guest on 18 February 2026

process between viruses and their hosts is also described by complex infection networks (Fortuna et al. 2010, Weitz et al. 2013, Edwards and Hayward 2024). A nested network is one of the hypothesized infection patterns resulting from gene-for-gene coevolution. In this process, viruses evolve to broaden their host range in response to increasing host resistance (Agrawal and Lively 2003, Dennehy 2012, Weitz et al. 2013). These complex interplays have been widely studied in the bacteria–phage model systems (Flores et al. 2011, Stern and Sorek 2011, Weitz et al. 2013) as well as in marine cyanobacteria and cyanophages (Waterbury and Valois 1993, Avrani et al. 2011, Zborowsky and Lindell 2019) and in microbial eukaryote–virus systems (Frickel et al. 2016, 2018, Edwards and Hayward 2024). Phytoplankton have developed various defence mechanisms and strategies to protect themselves against pathogens (Thomas et al. 2012). These strategies are diverse and include life-phase switch mechanisms (Brussaard et al. 2007; Frada et al. 2008; Frada et al. 2017), programmed cell death (Bidle 2016), lipidome plasticity (Schleyer et al. 2023), or spore formation (Pelusi et al. 2021). In the green microalgae *Ostreococcus* spp., antiviral resistance has been associated with changes in the size of small 'outlier' chromosomes (SOC), also known as 'immune' chromosomes, as well as in the transcription pattern of the latter (Thomas et al. 2011, Yau et al. 2016, 2018, 2020, Derelle et al. 2018). This chromosome encodes many predicted membrane-associated proteins, glycoconjugate production proteins important for host–virus interactions, and proteins associated with carbohydrate transport and metabolism, most of them being overexpressed in virus-resistant strains. In addition, these virus-resistant lines showed a reduction in the adsorption of viral particles on the surface of host cells (Yau et al. 2018).

Conversely, another important aspect is to better understand how these coevolutionary dynamics influence the adaptive response of viruses to spontaneous resistance in their hosts. The genus *Prasinovirus* belongs to the phylum *Nucleocytoviricota*, often referred to as 'giant viruses'. They infect cosmopolitan unicellular green algae of the class Mamiellophyceae, which includes the genera *Micromonas*, *Ostreococcus*, and *Bathycoccus* (Clerissi et al. 2012, Baudoux et al. 2015, Derelle et al. 2015, Bachy et al. 2021, Listmann et al. 2023), as well as the species *Mantoniella tinhauana* (Rey Redondo et al. 2024). Mamiellophyceae are widespread and dominate the eukaryotic picophytoplankton fraction in coastal waters (Tragin and Vaulot 2018, 2019). Their abundance supports dense populations of prasinoviruses, which are detected throughout marine environments where their hosts have been isolated (Cottrell and Suttle 1991; Cottrell and Suttle 1995; Zingone et al. 1999; Bellec et al. 2010). Metagenomic analyses further confirm that prasinoviruses are both widespread and abundant in the oceans (Short and Short 2008, Hingamp et al. 2013, Chen et al. 2018, Endo et al. 2020, Farzad et al. 2022, Ha et al. 2023). The global distribution of prasinoviruses and their hosts suggests a long-standing coevolutionary relationship. Indeed, *Prasinovirus*–Mamiellophyceae interactions exhibit a high degree of host specificity, with many viruses infecting only a single species or even specific strains within a species (Zingone et al. 2006, Clerissi et al. 2012, Bellec et al. 2014, Baudoux et al. 2015). These interactions are described as nested, wherein specialist viruses (narrow host range) and generalist viruses (broad host range) infect hosts that vary in their susceptibility or resistance to infection. Phylogenetic analyses of prasinoviruses and their hosts often showed congruent evolutionary trees, supporting the notion of virus–host coevolution (Bellec et al. 2014). While a strong co-speciation signal is observed in most *Prasinovirus*–Mamiellophyceae relationships, the *Bathycoccus*–virus system appears to reflect a more complex cophylogenetic history. This includes evidence for an early host switch from *Bathycoccus* to *Micromonas*, suggesting that prasinovirus colonization of *Micromonas* may be more recent (Bellec et al. 2014). Moreover, recent studies have uncovered unexpected host switching across diverse algal lineages, challenging existing paradigms of strict host–virus cospeciation (Thomy et al. 2024). These findings highlight the intricate evolutionary dynamics of the *Prasinovirus*–Mamiellophyceae system and underscore the importance of exploring the genetic mechanisms that govern host–virus interactions more broadly.

In this work, we used comparative genomic analysis of 18 distinct isolated viruses infecting *Ostreococcus tauri* (OtVs) and one infecting *Micromonas commoda*. We combined these results with cross-infections of a panel of distinct Mamiellophyceae strains to unveil the genetic signatures associated with OtV diversification and evolution of host range. Finally, the characterization of the infection dynamics and morphology of these viruses provided further insights into gene-to-phenotype associations.

Materials and methods

Culture of host algae and viruses

All algal cultures and viruses (Supplementary Fig. 1) were grown in liquid L1 medium (NCMA, Bigelow Laboratory for Ocean Sciences, USA) made with autoclaved offshore seawater (MOLA station: 42°27′11″N, 3°8′42″ E), diluted with Milli-Q water to give a final salinity of 35 PSU, and filter-sterilized through 0.22 μm polyethersulfone (PES) filters. The cultures were maintained at 15°C using a photoperiod cycle of 12-h:12-h light:dark (50 μmol photon m^{-2} s^{-1} white light).

Isolation of new viruses and host–virus specificity tests

Viruses from the Mediterranean Sea had been previously isolated between 2006 and 2009 (Clerissi et al. 2012). One virus from the North Sea and six viruses from the Pacific Ocean were isolated in this study. These viruses were isolated from half a litre of seawater collected from each marine station site (Supplementary Table 1) that was filtered through a 0.45-μm PES membrane filter (SARSTEDT reference; 83.1826), concentrated 10 times by tangential flow filtration (100-kDa PES Vivaflow200, Sartorius, Germany), and then, clonal viruses were procured by plating for individual plaques in exponentially growing *O. tauri* RCC4221 cultures, as described previously (Derelle et al. 2008). We considered that the virus strains were clonal after three successive infections of the host strain by the viruses from one lysis plaque. Fresh viral lysate was filtered through 0.22 μm or 0.45 μm pore-size filters to remove cellular debris and stored at 4°C in the dark. For host–virus specificity tests, a panel of Mamiellophyceae strains from the Roscoff Culture Collection (www.roscoff-culture-collection.org) (*O. tauri* RCC4221, RCC1123, RCC1117, RCC1116, RCC1110, RCC1115, RCC1108, RCC1114, RCC1561; *O. mediterraneus* RCC789; *M. commoda* RCC827; and *B. prasinos* RCC4222) were screened for their susceptibility to the viruses analysed in this study. Algal strains in exponential growth were incorporated into semi-solid L1 medium by addition of 1.5% molten agarose held at 58°C in a water bath (0.15% final concentration) and poured into Petri dishes (9 cm diameter). Three microliters of each viral lysate were deposited in duplicate on the surface of the semisolid medium for each algal strain, incubated at 20°C using a photoperiod of 12-h:12-h light:dark cycle (50 μmol photon m^{-2} s^{-1} white light), and the susceptibility to viral lysis was evaluated by the appearance of plaques visualized after 7 days.

Downloaded from https://academic.oup.com/ve/article/12/1/veaf096/8472608 by guest on 18 February 2026

Host–virus infection dynamics

Cross-infection assays were performed in a 96-well cell culture plate (200 μl final volume) in triplicate using a host cell concentration of 10^6 cells/ml and 10^7 viral-like particles/ml of virus (virus-to-host ratio of 10). Viral particle concentration was measured at the final time point and compared to the known concentration at time zero. The plate was incubated at 20°C using a photoperiod cycle of 12-h:12-h light:dark (50 μmol photon m^{-2} s^{-1} white light). The growth of the host cells was monitored using chlorophyll *a* autofluorescence (excitation/emission: 430/670 nm) in a Victor Nivo microplate reader over 15 days. To estimate the number of virus-like particles produced during infection, all the viral lysates were collected, and the concentration of viruses was measured by flow cytometry at the end of the 15 days of the experiment, as described by Brussaard (Brussaard 2004). Briefly, viruses were fixed with 0.5% glutaraldehyde (25% electron microscopy grade) for 15 min and flash-frozen and stored at −80°C until measured. Virus particles were thawed, diluted in Tris-EDTA (TE) buffer (pH = 8.2, 10 mM Tris–HCl, 1 mM ethylenediaminetetraacetic acid (EDTA) filtered through 0.02 μm pore-size filters (Anotop syringe filter, Whatman) marked with SYBR-Green (10^{-5} dilution of stock, Thermo Fisher Scientific) by heating to 80°C in the dark for 10 min. Virus particles were enumerated in the CytoFLEX flow cytometer (Beckman Coulter) gated on green fluorescence versus side scatter. *Ostreococcus* growth rate in the re-growth exponential phase was calculated as the slope of log(concentration) regression. Re-growth exponential phase corresponds to the phase where the *Ostreococcus* growth rate becomes positive after the culture reaches its minimum concentration and before reaching the saturation phase again. If necessary, we removed points at the border of the re-growth exponential phase to ensure estimating the maximum growth rate using the best possible regression fit that minimizes the error between the model and the data.

Transmission electron microscopy

Observation of viral particles in negative staining was performed on copper grids coated with Formvar film and carbon film (FCF200-Cu—EMS), rendered hydrophilic by effluviation (20 s of air glow discharge, -ve, GloQube® Plus Glow Discharge System). The grid was inverted onto a drop of fresh 0.45 μm-filtered viral lysate for 30 min to allow viruses to adhere to the grid support film. After removal of excess sample by adsorption onto filter paper, the grid was laid on a drop of 2% aqueous uranyl acetate solution for 45 s. After absorbing the excess dye with filter paper, the grid was air-dried. The observation was performed on a Hitachi 7500 transmission electron microscopy (TEM).

For thin-section observation by TEM, noninfected (control) and infected *O. tauri* cells (infected with OtV09-565) were prepared following the protocols of Chretiennot-Dinet et al. (Chrétiennot-Dinet et al. 1995) and Derelle et al. (Derelle et al. 2008). A concentration of 15×10^6 cells/ml, contained in 50 ml aliquots of samples prefixed with 1% glutaraldehyde (Electron Microscopy Sciences), was collected by centrifugation at 2500 × *g* for 30 min. The pelleted cells were then quickly mixed with 40 μl of low-melting-point agarose (Sigma) at 37°C using a micromanipulator (SMI, Emeryville, CA, USA). Once the agarose solidified, the agar block containing the cells was fixed for 2 h at 4°C in 2.5% glutaraldehyde prepared with one volume of 0.4 M cacodylate buffer and two volumes of culture medium (L1 medium) and washed three times for 15 min each in one volume of 0.4 M cacodylate buffer and one volume of culture medium. Post-fixation was carried out in 1% osmium tetroxide (OsO_4) (Electron Microscopy Sciences) in 0.2 M cacodylate buffer for 1 h. After two washes in the same buffer, the small agar blocks were gradually dehydrated in ethanol (70%, 95%, 100%), then infiltrated and embedded in Epon 812 resin (Electron Microscopy Sciences). Ultrathin sections (80 nm) were obtained using an ultramicrotome (Leica Ultracut R) and examined on a Hitachi 7500 TEM after staining with uranyl acetate and lead citrate. The resulting images were processed using ImageJ software.

Partial DNA polymerase B gene amplification and sequencing

We determined that the newly isolated viruses were prasinoviruses based on polymerase chain reaction (PCR) screening of the partial *polB* gene, which is a viral marker gene, using the primer sets in Clerissi et al. (2014). PCR reactions were done as follows: 2 μl of fresh viral lysate was added to 48 μl of reaction mixture containing 1× PCR buffer, 1 mM $MgCl_2$, 0.2 mM deoxyribonucleoside triphosphate (dNTP) mix, 0.5 μM of each primer, 0.1 $mg.m^{-1}$ bovine serum albumin (BSA), and 1.25 U of Taq DNA polymerase (GOTaq® G2 Flexi M7805, Promega). PCR was performed in a Mastercycler Nexus system (Eppendorf) using an initial denaturation at 95°C (3 min), 38 rounds of denaturation at 95°C (30 s), annealing at 49°C (60 s), extension at 72°C (3 min), and final extension at 72°C (4 min). PCR products were loaded into a 0.8% agarose electrophoresis gel in 0.5% TAE (Tris-acetate-EDTA) buffer and visualized under ultraviolet light after ethidium bromide staining. Before Sanger sequencing, PCR products were purified using a Wizard® SV gel and PCR clean-up system kit (Promega, ref A9281). Sequences were cleaned by manually trimming low-quality base pairs from the 3′ and 5′ ends using Geneious Prime (version 2.1) (https://www.geneious.com). We ensured the identity of the four *O. tauri* strains (RCC4221, RCC1116, RCC1108, RCC1123) by amplification of variable regions of chromosome 20 by PCR consisting of F36 (5′-TCG ACG CAC CTT TTC CCC-3′) and R641 (5′-CGA CGA CGA CGC TCG AAC-3′) primers.

Concentration and purification of viral particles

A total of 2 L of viral lysate from each strain was produced and filtered through a 0.2 μm PES membrane filter (SARSTEDT, ref 83.1826) to remove cellular debris and bacteria. Viral particles filtered were concentrated 40-fold by tangential flow filtration using a 100 kDa molecular weight cut-off (MWCO) PES membrane Vivaflow200 unit (Sartorius, Germany, ref VF20P4). We concentrated the filtered lysate a second time with a 50 000 MWCO PES membrane Vivaspin20 ultracentrifugation unit (Sartorius, Germany, ref VS2031). Viral particles were further purified in an iodixanol (Optiprep™, Sigma-Aldrich, ref D1556) density gradient by ultracentrifugation rotor (SW41 Ti rotor, Beckman Coulter) at 175 117 × *g* for 5 h at 4°C. For each virus, a single visible band in the 30% fraction, corresponding to the purified concentrated viral particles, was collected and pelleted by ultracentrifugation at 245 000 × *g* for 2.5 h at 4°C (SW55Ti rotor, Beckman Coulter). The virus pellets were resuspended in a sterile Saline-Magnesium (SM) buffer (100 mM NaCl, 8 mM MgSO4-7H2O, 50 mM Tris pH 7.5) and stored at 4°C.

Extraction and sequencing of viral DNA

DNA was extracted from the purified viruses with the Cetyl-Trimethyl-Ammonium Bromide buffer (CTAB) protocol, as previously described (Winnepenninckx et al. 1993) with the following modifications. After CTAB buffer incubation (65°C for

Downloaded from https://academic.oup.com/ve/article/12/1/veaf096/8472608 by guest on 18 February 2026

30 min), an equal volume of phenol:chloroform:isoamyl alcohol (25:24:1) was added, and the samples were centrifuged (15 000 × *g* for 10 min at 4°C). The aqueous phase was recovered, mixed with an equal volume of chloroform:isoamyl alcohol (24:1) and centrifuged (15 000 × *g* for 10 min at 4°C). Two litres of RNAse A (1 M) (DNase free) was added to the aqueous phase for 30 min at 37°C, and then, the enzymes were inactivated by heating for 10 min at 60°C. One-tenth volume of ammonium acetate (3 M, pH 5.3) was added to favour DNA precipitation. Nucleic acids were precipitated using 2.5 volumes of absolute ethanol, gently homogenized and transferred at −80°C overnight. The precipitated DNA was centrifuged at 15 000 × *g* for 30 min at 15°C and the pellet was washed in 70% ethanol. Finally, the samples were centrifuged (15 000 × *g* for 10 min at 15°C), air-dried, and DNA dissolved in 50 μl of DNAse/RNAse-free water and stored at 4°C. DNA in 1 μl was quantified by fluorimetry (Quantus™) using the QuantiFluor® dsDNA system kit (Promega, ref E2670).

Viral DNA (1 μg) was submitted to Illumina NEXTFLEX library preparation (average insert size 241 bp) and sequenced using Illumina NextSeq 550 technology in paired-end mode (2 × 150 bp), giving a yield of 120 million reads total. Reads were cleaned with Trimgalore software (v0.6.5) (Krueger 2012) (with options –paired –fastqc –illumina –quality 26 –stringency 3 –length 35 –three_prime_clip_R1 10 –three_prime_clip_R2 10 –clip_R1 10 –clip_R2 10), and the read quality was evaluated with FastQC (v0.11.7) (Andrews 2010) with default settings.

De novo genome assembly

We found that optimal *de novo* assembly of viral genomes required read data down-sampling, as using the entire dataset with an estimated coverage of 6000× induced assembly fragmentation. Down-sampling was performed using the tool seqtk version 1.3 (Li 2012). A total of eight independent sets of randomly down-sampled reads (seed numbers 100) were obtained, given a coverage of 5×, 10×, 50×, 75×, 100×, 500×, 1000×, and 2500× for each virus genomic library. *De novo* assembly was performed using Spades (v3.15.1) (Bankevich et al. 2012) all sets of independently down-sampled reads, as well as for the total set of cleaned reads. To ensure optimal assembly, and since some samples were revealed to have two independent viruses, we further assessed two assembly options: '–isolate' and '–meta'. The 18 assemblies for each viral strain were compared, and the choice of the 'best' assembly was based on optimizing for three quality criteria given by QUAST (v5.0.0) (Gurevich et al. 2013). Specifically, we sought to maximize the size of the longest contig and to reduce ambiguous nucleotide positions (lowest number of *N*'s) and the total number of contigs. To facilitate the comparative genomic analysis, genomes comprising several contigs were manually scaffolded using Geneious (v11.0.3 + 7) (https://www.geneious.com), to ensure that the order of genes was conserved relative to that of viral genomes that were assembled as a single contig. The reads were mapped to the final genome assembly with the Burrows–Wheeler Aligner (BWA v0.7.17) using maximum exact matches (BWA-MEM) and a minimum seed length of 20 while keeping the other default parameters to further assess a correct assembly (Li and Durbin 2009). Specifically, we verified that re-mapped read depth was even along the length of the genome.

Gene prediction and functional annotation

Gene prediction of OtV genomes was performed using Prokka (v1.14.5), specifying 'virus' as the taxonomic kingdom (Seemann 2014). First, protein-coding genes (CDS) were annotated using the databases implemented in Prokka with the following parameters: e-value, 1e-5; and genetic code, standard (–gcode 1). Secondly, transfer ribonucleic acids (tRNAs) were predicted using tRNAscan-SE with default parameters (v2.0.2) (Chan and Lowe 2019). Thirdly, additional functional annotation of all protein sequences was sought by BLASTp search against the National Center for Biotechnology Information (NCBI) nr database, accepting an e-value of <1e-5, keeping only the best hit. Finally, taxonomic affiliation was associated with each protein accession using Entrez Direct (EDirect) (epost -db protein | esummary -db protein | xtract -pattern DocumentSummary -element Caption,TaxId) (Kans 2021).

Structural predictions of single protein sequences from OtV genomes' hypervariable regions were conducted with AlphaFold3 on the server https://alphafoldserver.com/ (version AlphaFold-beta-20 231 127) (Abramson et al. 2024) with automated seed and otherwise standard parameters. Per-atom confidence estimates are recorded as pLDDT in the b-factor column of CIF files, with regions of pLDDT > 90 representing very high confidence and regions of pLDDT < 50 representing very low confidence. The best-ranking PDB model for each target was then submitted to Foldseek structural similarity search on the server https://search.foldseek.com/search through all available databases (AlphaFold/Proteome, AlphaFold/Swiss-Prot, AlphaFold/UniProt50, CATH50, GMGCL, MGnify-ESM30, PDB100) in 3Di/AA mode (van Kempen et al. 2024). Most significant explicit descriptions of each target function were chosen based on the coverage of alignment of target and query, the statistical e-value of alignment, and Foldseek self-consistency between databases.

Comparative genomic analysis

The complete genomes of the previously available prasinoviruses were downloaded from NCBI (Supplementary Table 2). A total of 36 genomes (19 new sequence genomes and seventeen prasinovirus references) were used to define groups of orthologous genes (orthogroups), where we excluded prasinovirus reference genomes that were incomplete or too fragmented (i.e. BII-V1, OlV3, OlV4, OlV5, and OlV6). All translated CDSs were included in the orthogroup analysis using Orthofinder with default settings (Emms and Kelly 2019). Each orthogroup was annotated *via* the EggNOG-mapper toolkit (v2.0.4-rf1) against EggNOG protein database (-m diamond) using the setting parameters (Huerta-Cepas et al. 2017). The Euclidean distance between the viruses based on the presence/absence pattern of orthogroups was calculated using pvclust R package (v2.2-0) based on the 'ward.D2' hierarchical clustering linkage method, and approximately unbiased (AU) *P*-values are computed using 1000 bootstrap replicates (default settings). Orthogroup distribution in each genome was represented using the pheatmap R package (v1.0.12). Pairwise whole-genome alignments of OtVs were carried out using pyGenomeViz v1.0.0 with default parameters (https://github.com/moshi4/pyGenomeViz), and pgv-pmauve, part of pyGenomeViz, was used for visualization of genome alignment with 'nucleotide method' as setting parameters. Average Nucleotide Identity (ANI) between all orthologous genes shared between all pairs of OtV genomes was computed using FastANI (v.1.32) (Jain et al. 2018). Genomic maps of the hypervariable region between specialist and generalist viruses were generated using Easifig (v2.2.2) (Sullivan et al. 2011).

K_a/K_s ratio calculation

The ratio of nonsynonymous (K_a) to synonymous (K_s) substitutions of the targeted coding sequences in the HVR was computed

Downloaded from https://academic.oup.com/ve/article/12/1/veaf096/8472608 by guest on 18 February 2026

using KaKs_Calculator2.0 (D. Wang et al. 2010). For this purpose, the ratio was estimated across different alignments for genes with sequences of >80% nucleotide identity. The KaKs_Calculator2.0 was run on each nucleotide alignment group separately through different methods (option: -m MA, MYN, LPB, MS, and NG). The value of the ratio was deemed reliable if the models compared gave the same score, and the method with the highest *P*-value was then selected.

Phylogenetic analysis

Phylogenetic reconstruction based on full-length DNA polB protein and 19 core proteins (the list of the core proteins is found in Supplementary Table 8) shared between *Prasinovirus* and *Chlorovirus* genomes was performed. Protein sequences were aligned using MAFFT (v.7.313) with the L-INS-i algorithm (Katoh et al. 2002). We trimmed each alignment, removing positions containing >80% gaps with Goalign (v0.3.2) (Lemoine and Gascuel 2021). Phylogenetic trees of single proteins and concatenated proteins (comprising 5483 amino acid positions) were built using the Maximum-Likelihood (ML) method with IQ-TREE version 2.0.6 (Minh et al. 2020). For mixture model analysis, the LG+F+R4, LG+R3 and LG best models were chosen (option -m MFP) according to the Bayesian information criterion (BIC) for concatenated proteins and full-length DNA polB protein, respectively (Kalyaanamoorthy et al. 2017). The branch support values were computed from 1000 replicates for the Shimodaira–Hasegawa (SH)–like approximation likelihood ratio test (aLRT) (Guindon et al. 2010) and 1000 ultrafast bootstrap approximation (UFBoot) (Hoang et al. 2018). The trees were visualized with Interactive Tree Of Life (iTOL) v6 (Letunic and Bork 2007).

Results

Newly isolated prasinoviruses from distant geographic origins

We sought to expand the diversity of marine viruses in our study group by isolating new viruses from distant sites across the globe. Nine taxonomically diverse eukaryotic phytoplankton strains (Trebouxiophyceae, Mamiellophyceae, Pyramimonadophyceae, and Pavlovaceae) were challenged with environmental seawater from two distant coastal sites (South Pacific Ocean Gyre and South in the Eastern North Sea) (Supplementary Table 1). No lytic viruses were detected for Trebouxiophyceae, Pyramimonadophyceae, and Pavlovaceae strains in our culture conditions using the volumes of seawater tested. The viral titres in the seawater samples were sufficient to lyse only the Mamiellophyceae strains of the genera *Micromonas*, *Ostreococcus*, and *Bathycoccus*. We successfully isolated viruses on *O. tauri* RCC4221 and *M. commoda* RCC827 strains from seawater sampled from three distinct sites in the Pacific Ocean along the Chilean coast and from the North Sea (Supplementary Fig. 1). Overall, we isolated six new viruses infecting *O. tauri* and one infecting *M. commoda* (Supplementary Fig. 1).

PCR amplification of the viral DNA polymerase B gene (*polB*) with degenerate primers and Sanger sequencing supported the taxonomic affiliation of these viruses to the genus *Prasinovirus*. Genomes of these seven new prasinoviruses, along with those of 12 genetically distinct OtVs previously isolated from the coastal Mediterranean Sea (Clerissi et al. 2012), were sequenced to extend our knowledge of prasinovirus diversity.

Genomic features of prasinoviruses

Nineteen new prasinovirus genomes were successfully assembled from Illumina high-throughput sequences, all of which were found to be linear double-stranded DNA genomes of ~190 kb (Supplementary Table 2). From the OtV19-T viral lysates, two separate contigs were successfully recovered with a length of 189 and 200 kb and with a GC composition of 41.9% and 41.2%, respectively. On each of these contigs, different *polB* genes were present in a single copy, suggesting a co-infection of two distinct viruses (dubbed OtV19-T1 and OtV19-T2) on the same host. The presence of two viral genomes was surprising, as all viruses were isolated by picking off individual virus plaques through three successive rounds of plating. One possibility is that the plaque purification was insufficient to separate them, for example, if the virus particles were closely physically associated such that they were copurified. Another possibility is that these two genomes might be defective for unknown different but complementary functions and require coinfection to reproduce.

While most viruses described in this study presented a highly similar genome length, comparable with the other *Ostreococcus* virus reference genomes, some of them (4 out of 18 viruses) displayed a significantly different DNA base composition (GC content) and a higher number of coding DNA sequences (CDS), separating them into two main groups (Supplementary Fig. 2). The first group includes most of the viruses, such as those from the Mediterranean and North Seas. This group encodes ~247 CDSs with a GC content of 45%. The second group, which includes mainly viruses from the Pacific Ocean (four out of five), was distinguished by a higher number of CDSs (260) and a lower GC content (41%). Its genetic features were more closely allied to those of the newly isolated *Micromonas* virus (McV20-T) (see Supplementary Fig. 2). All OtVs and McV20-T encode a *polB* gene as well as seven to nine copies of major capsid protein (MCP) genes, depending on the strain. Although all MCP genes are identifiable as capsids by amino acid sequence similarity to structurally described capsid proteins and by their structural prediction (double-jelly roll fold), each capsid gene is clearly separated by its nucleotide sequence divergence (Supplementary Table 3) that places it in a different cluster (Supplementary Fig. 3). Phylogenetic analysis of the protein capsids found in all prasinoviruses suggests that the capsid gene copy expansion occurred in the common ancestor of *Prasinovirus* and *Chlorovirus* genera, as the phylogeny of the MCP shows a similar topology in a comparison between eight prasinovirus genomes infecting host genera *Ostreococcus*, *Micromonas*, and *Bathycoccus* (Clerissi et al. 2014). Furthermore, our analysis shows the ninth copy of MCP observed in both OtV06-12 and OtV19-T2 viruses resulted from a duplication event from the MCP1 gene that occurred during evolution. While the detailed molecular architecture of a *Prasinovirus* virion is yet to be elucidated, we hypothesize that all capsid genes are used to form the virion, as in the model algal chlorovirus, PBCV-1, which encodes seven capsid genes from five paralogous groups and is the closest relative of *Prasinovirus* that has its virion structure resolved (Nandhagopal et al. 2002, Shao et al. 2022).

A greater number of tRNA genes are also identified in OtV19-O, OtV19-P, OtV19-T1 (8 tRNAs) as well as in OtV6 (9 tRNAs) compared to other viruses that harbour approximately five tRNAs (Supplementary Table 2). Although five tRNAs ($tRNA_{Gln}$, $tRNA_{Ile}$, $tRNA_{The}$, $tRNA_{Asn}$, and $tRNA_{Tyr}$) were found to be common to all OtVs (except OtV1), two ($tRNA_{Arg}$ and $tRNA_{Pro}$) were unique to these four viruses (OtV19-O, OtV19-P, OtV19-T1, and OtV6). Furthermore, some of these ($tRNA_{Gln}$, $tRNA_{Tyr}$, $tRNA_{Asn}$,

Downloaded from https://academic.oup.com/ve/article/12/1/veaf096/8472608 by guest on 18 February 2026

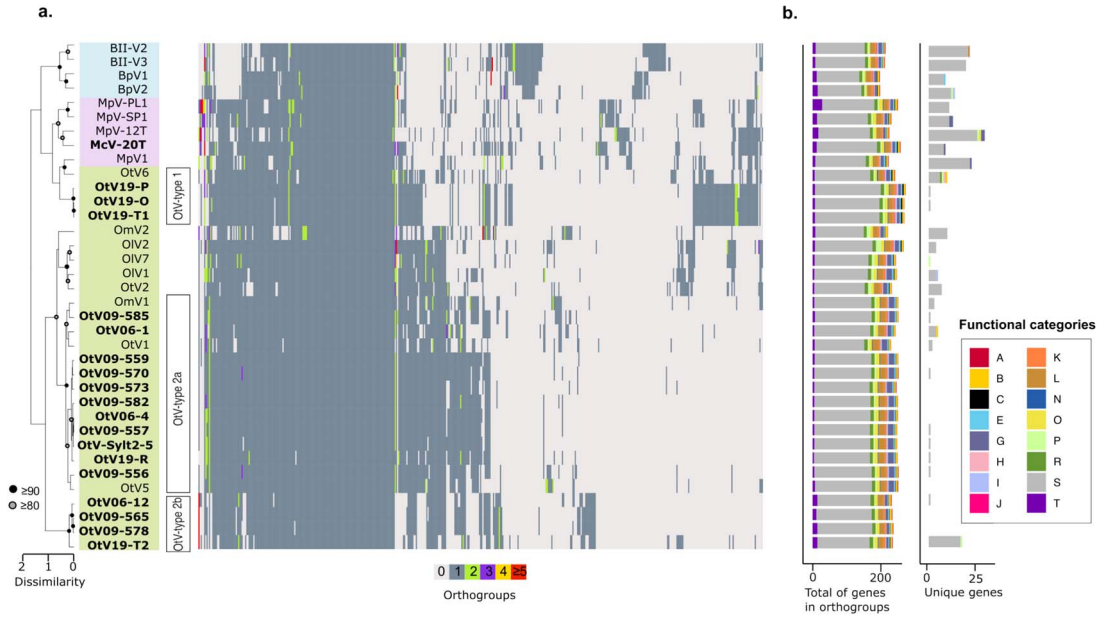


Figure 1. Orthologous protein distribution of prasinoviruses. (a) Heatmap showing the distribution and frequency of all orthogroups in *Bathycoccus*, *Micromonas*, and *Ostreococcus* viruses. Virus names in bold were sequenced in this study. The heatmap was ordered vertically by hierarchical clustering of viral genomes based on the occurrence pattern of all orthogroups (left dendrogram) and horizontally by clustering of the orthogroups based on their distribution in the viral genomes. Nodes marked with a grey dot show genome clusters with over 80% bootstrap support, and black dots show over 90% support. (b) Bar charts showing (left) the total number of genes assigned to an orthogroup and (right) the number of unique genes (not shared with any other virus analysed) in each viral genome. Bar charts colored according to the distribution of functional categories based on the EggNOG database.

and $tRNA_{Thr}$), were found to be clustered together near the 3′ end of the genome. tRNA clusters have already been reported in chlorovirus, as well as in prasinovirus genomes (Moreau et al. 2010, Duncan et al. 2020). Hierarchical clustering based on the presence and absence pattern of tRNA genes shows a close relationship between the three OtV19-O, OtV19-P, and OtV19-T1 viruses and OtV6 (Supplementary Fig. 4). Likewise, viruses within the same cluster showed synteny of tRNA genes in their genomes. The acquisition and selection of specific tRNAs might enable viruses to adapt to codon usage bias for the synthesis of their own proteins by complementing the pool of tRNAs available from their host cell (Michely et al. 2013, Azam et al. 2024), or it might reflect viral adaptations to host defence mechanisms (Zborowsky et al. 2025, Sirihongthong and Auewarakul 2025). It is therefore possible that these three new viruses isolated from the Pacific Ocean and OtV6 infect a host with a distinct codon usage bias from *O. tauri* in the environment. Finally, terminal inverted repeats (TIRs) were identified from most OtV viruses (16 out of 18) as well as in the McV-20 T (Supplementary Table 2), indicating the successful assembly of these genomes. While the biological role of TIRs during infection remains poorly understood, these features appear to be commonly found in prasinovirus genomes (Derelle et al. 2008, Bachy et al. 2018, 2021, Rey Redondo et al. 2024).

Distinct evolutionary relationship and gene composition

Phylogenetic reconstruction based on DNA polB and concatenation of 19 core proteins places the isolated viruses as new members of *Prasinovirus* (Supplementary Fig. 5), which is classified within the order *Algavirales* based on other phylogenetic frameworks (Aylward et al. 2021). The resulting phylogenetic tree places McV20-T within the paraphyletic clade containing *Micromonas* viruses (MpV1, MpVSP1, MpVPL1), while the OtVs within the large cluster of viruses infecting *Ostreococcus* form a monophyletic group (Supplementary Fig. 5).

Hierarchical clustering based on the orthogroup pattern (Fig. 1) reveals a topology comparable to the multi-protein phylogenetic tree with OtVs separated into two clades (Supplementary Fig. 5), with the exception that *Ostreococcus* viruses do not form a single large cluster. In contrast, the orthogroup analysis permits separation of OtV groups according to other factors shaping the noncore genes or pan-genome, which potentially include specific environmental or host-interacting genes. Hence, based on both genome-wide diversity (Fig. 1) and the evolutionary relationships (Supplementary Fig. 5), three main OtV groups were defined. The first one dubbed OtV-type 1 includes the three Pacific Ocean viruses (OtV19-O, OtV19-P, and OtV19-T1) and OtV6, which form a large cluster within the *Micromonas*-infecting viruses clade. The second group was segregated into two distinct subgroups: OtV-type 2a and OtV-type 2b. OtV-type 2a comprises all OtVs (except OtV2, whose host species was not *O. tauri*, but *Ostreococcus* sp. clade B; Weynberg et al. 2011) and the *O. mediterraneus* virus 1 (OmV1), while OtV-type 2b comprises the fast-diverging strains OtV06-12, OtV09-565, OtV09-578, and OtV19-T2 (Fig. 1).

Pan-genomic analysis revealed that 37 of the 482 orthogroups were present in all prasinovirus genomes (core orthogroups) (Supplementary Table 4). The large *Ostreococcus* virus clade shared a total of 118 core orthogroups, while 136 were found in *Micromonas* virus and 134 in *Bathycoccus* virus genomes. A total of 139 core orthogroups were found among the three newly defined OtV groups. Based on the EggNOG classification, only around 28% of the genes were assigned to putative functions. Most of them were associated with RNA processing and modification, amino acid metabolism and transport, nucleotide metabolism and transport, lipid metabolism, and DNA replication/repair (Fig. 1). Among the *O. tauri* virus clade, OtV-type 1 was the most distinct group with 43 unique orthogroups and 25 of which were present in at least one *Micromonas* virus genome, representing ~60% of

Downloaded from https://academic.oup.com/ve/article/12/1/veaf096/8472608 by guest on 18 February 2026

the orthogroups in this group (Supplementary Table 4). Of all these genes, only six encode known functions, such as a mannitol dehydrogenase C-terminal domain protein, a glycerophosphoryl diester phosphodiesterase family protein, a mitochondrial 18 kDa protein and an alternative oxidase (AOX), a copper/zinc superoxide dismutase, and an endosialidase chaperone. Finally, OtV-type 2a and OtV-type 2b share 6 and 11 unique orthogroups, respectively. Interestingly, within OtV-type 2b, two signature genes were annotated as glycosyltransferase family 17 and a coiled stalk of trimeric autotransporter adhesin, both involved in host interaction and immune evasion.

The OtV genome is modular, comprising syntenic and variable regions

Overall, the genomes of OtVs displayed a high collinearity and gene synteny (Fig. 2). The pairwise average nucleotide identity (ANI) values between them ranged from ~71% to 99%, indicating a very low level of divergence (Supplementary Table 5). The organization and structure of gene function followed a genomic pattern of locally collinear blocks (LCBs) (Darling et al. 2004), which define homologous regions of sequence shared by the genomes (Fig. 2). The first two LCBs (LCB1 and LCB2) included a broad range of genes associated with carbohydrate, nucleotide, and amino acid biosynthesis and metabolism. The LCB3 and LCB4 included genes with functions involved in adhesion, cell recognition, and morphogenesis. The central LCBs (5–9) were very conserved among the prasinoviruses and contained the bulk of the core genes associated with DNA transcription, replication, and post-transcriptional modification. The LCB10 and LCB11 encode genes involved in amino acid and polysaccharide synthesis and metabolism, while the last four blocks also contained genes associated with DNA replication and morphogenesis including two capsid genes and DNA polymerase B and DNA topoisomerase II. In addition, some glycosyltransferases, associated with carbohydrate biosynthesis and metabolism, were found in these regions.

Minor LCBs, not shared by all viruses, were observed at the genome extremities (Fig. 2). These regions, called virus-specific regions (VSRs), harbour genes only present in certain OtV-types. The first VSR (VSR1), spanning ~20 kilobases (kb), was present in all viruses except OtV-type 2b (Supplementary Fig. 6a). Most of these genes had functions associated with carbohydrate metabolism, such as glycosyltransferase, galactotransferase, thiamine pyrophosphate enzyme, Nicotinamide Adenine Dinucleotide (NAD)-dependent epimerase/dehydratase, Guanosine Diphosphate (GDP)-mannose 4,6 dehydratase, and other genes more associated with fatty acids, amino acids, and secondary metabolism. The second VSR (VSR2) consists of two separated blocks encoding a total of 23 genes, which were only found in the three virus genomes associated with the OtV-type 1 (OtV19-O, OtV19-P, OtV19-T1) (Supplementary Fig. 6b). Among these genes, only seven (30%) encode a known function, namely, DNA polymerase X family, staphylococcal nuclease homologue, mitochondrial 18-kDa protein, mannitol dehydrogenase, 2OG-Fe(II) oxygenase, AN1-like Zinc finger, and deoxycytidylate deaminase. These genes are associated with nucleotide transport and metabolism, replication, recombination and repair, carbohydrate metabolism, and other diverse functions. Interestingly, highly similar homologs of these genes were also identified in *Micromonas* viruses. Phylogenetic analysis of the mitochondrial 18-kDa protein indicates a recent lateral transfer of this gene between green algae and viruses (Supplementary Fig. 7).

We identified a large non-homologous region between positions 25 and 80 kb of the genomes (from LCB3 to LCB5) (Fig. 2). This region, hereby described as hypervariable (HVR), was characterized by complex rearrangements (i.e. deletions, duplications, acquisitions) of genes primarily associated with adhesion and cell recognition functions (Supplementary Fig. 6a), as well as morphogenesis, such as capsid proteins. A notable feature of this HVR was its expansion in OtV-type 2b viruses, which formed a faster diverging branch in the phylogenetic analysis (Supplementary Fig. 5).

The hypervariable region is a hotspot of host interaction genes

The HVR was characterized by a strong decrease in nucleotide sequence identity between viruses of different types and higher identity between the viruses of the same OtV-type, except for viruses of OtV-type 2b that showed large structural variations (Supplementary Fig. 6a). The HVR is flanked by homologous core genes (from LCB3 and LCB5). Two capsid proteins delimited it on either side, and a third capsid protein was found in the central part, except for OtV06-12 and OtV19-T2 that encoded a fourth homolog (Fig. 3).

Upstream of the HVR were genes with functions associated with various biological functions, such as a DEAD-like helicase protein, an ABC1 atypical kinase-like domain-containing protein, an NAD(P)-binding Rossman-like domain-containing protein, and a 2OG-Fe(II) oxygenase. In addition, a putative potassium ion (K+) channel protein was also identified in the region upstream of the HVR. The K+ channel gene was identified exclusively in OtV-type 1 (i.e. OtV19-P, OtV19-T1, OtV19-O, and OtV6) and in all *Micromonas* viruses including the newly characterized McV20-T (Supplementary Fig. 7). Furthermore, homologs were identified in the *Ectocarpus* virus and its host with a high identity (94.4%). Phylogenetic reconstruction of the K+ channel protein places prasinoviruses, chloroviruses, and Tetraselmis virus 1 (TetV-1) within a single monophyletic group with the filamentous brown alga *Ectocarpus siliculosus* and its virus (Supplementary Fig. 8). While the evolutionary history of K+ channel protein seems difficult to assess between prasinoviruses and their hosts, our analysis indicated a recent lateral gene acquisition between *E. siliculosus* virus and its host (Supplementary Fig. 8). Interestingly, in OtV-type 2, a transmembrane protein with a distinct function was detected at the same genomic locus where the K+ channel gene was found in OtV-type 1 (Fig. 3a), suggesting a likely evolutionary divergence of this gene between OtV-types.

The region downstream of the HVR consists of genes mainly associated with replication, recombination and DNA repair (i.e. prim-pol4 protein), as well as other functions such as NUDIX hydrolase domain protein, DUF5775 domain protein. Within the HVR, although most genes had unknown functions, most of the others were involved in cell recognition, adhesion, and morphogenesis. For OtV-type 1 and OtV-type 2a, these were predicted to be cell wall surface anchor family proteins (FhaB) and found in multiple copies. A phage tail assembly chaperone protein was identified in the OtV-type 1, as well as in one virus from OtV-type 2a (OtV09-559) and two viruses from OtV-type 2b (OtV06-12 and OtV19-T2). In addition, a chaperone endosialidase was predicted only in the OtV06-1, OtV09-585, OtV09-570, and OtV09-556 genomes. A remarkable feature of the HVR is its substantial expansion in the OtV-type 2b, which is more than three times longer than that of other viruses (Fig. 3). For example, the average length is 15 kb in OtV-type 1 and OtV-type 2a, compared to ~40 kb in OtV-type 2b (Fig. 3). This difference in size was notably associated with

Downloaded from https://academic.oup.com/ve/article/12/1/veaf096/8472608 by guest on 18 February 2026

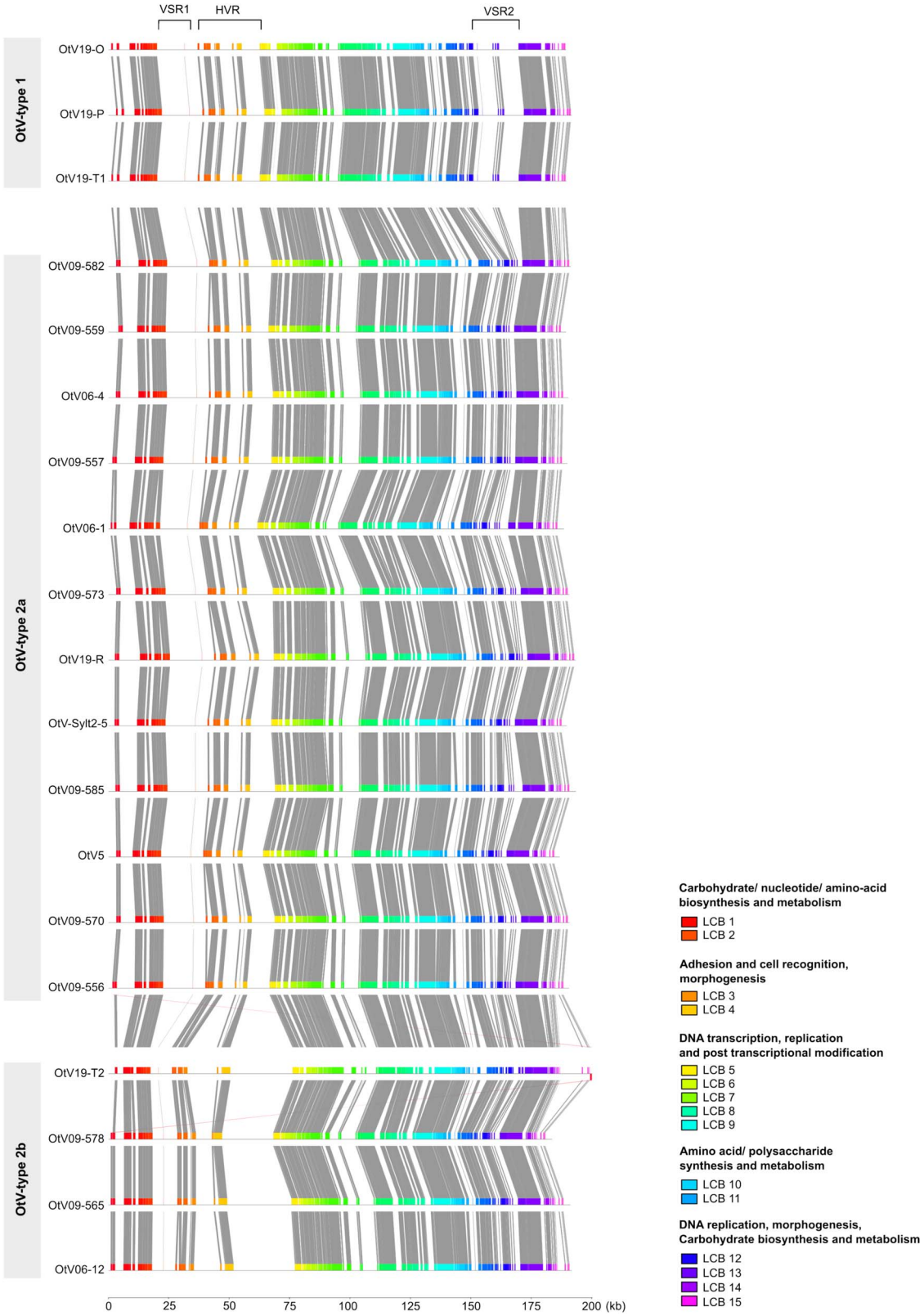


Figure 2. Comparison of the full-length genomes of *O. tauri* viruses. Colored blocks correspond to conserved regions that are locally collinear and homologous between viral genomes. Such segments are referred to as locally collinear blocks (LCBs) and connected by the lines and indicate commonly conserved regions between all genomes. The genomes are sorted by OtV-types (OtV-type 1, OtV-type 2a, and OtV-type 2b). The scale is indicated in kilobase (kb). VSR, virus-specific region; HVR, hypervariable region.

Downloaded from https://academic.oup.com/ve/article/12/1/veaf096/8472608 by guest on 18 February 2026

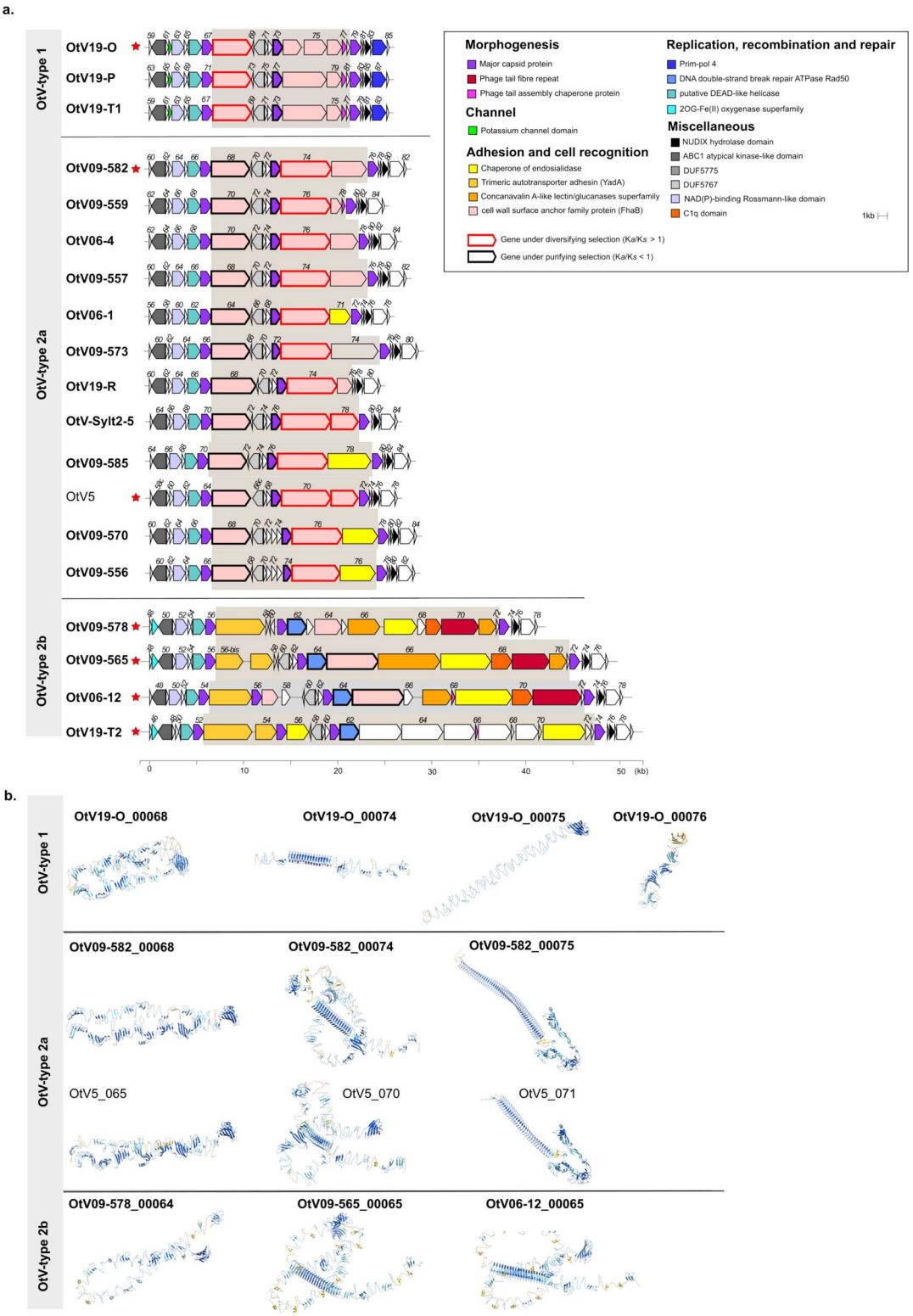


Figure 3. Description of the hypervariable region in OtV genomes. (a) Genomic map comparing a partial sequence in which the hypervariable region was detected in the OtV genomes. The hypervariable region is delimited by the box. The OtV5 genome (unbolded) was used as a reference genome. Genomes were sorted according to their OtV-type based on their phylogenetic relationship and gene family composition (OtV-type 1, OtV-type 2a, and OtV-type 2b). Stars indicate viruses for which the search for gene function and/or conserved domain and structural domains was performed and then have been used as a reference for each OtV-type (Supplementary Table 7). Homologous genes were colored identically according to their functional categories. White open reading frames have no predicted function. Each open reading frame was numbered according to its associated locus tag. BLASTn comparisons between the OtV06-12, OtV09-578, OtV09-565, OtV19-T2, OtV5, OtV09-582, and OtV19-O genomic regions are shown in Supplementary Fig. 5. The scale bar indicates the length of the genomic region in kilobases (kb). Genes under positive selection (K_a /K_s > 1) are bolded and framed, while those under purifying selection (K_a /K_s < 1) are bolded and framed. (b) The three-dimensional (3D) structure of the cell wall surface anchor family protein (FhaB) associated with hypervariable regions in the OtV genomes. OtV06-12, OtV09-578, OtV09-565, OtV5, OtV09-582, and OtV19-O were used as a reference for each type. Viruses isolated and sequenced in this study are bolded. A close-up view of β-folded segments of the FhaB protein is shown in Supplementary Fig. 12. The full structural protein is shown in Supplementary Fig. 12.

Downloaded from https://academic.oup.com/ve/article/12/1/veaf096/8472608 by guest on 18 February 2026

the acquisition of unique genes that are most likely involved in host interaction and recognition. These genes encode phage tail fibre proteins, concanavalin A-like lectin/glucanase superfamily proteins, and trimeric autotransporter adhesins (YadA). In addition, a gene with a putative C-terminal Rad50 domain protein, located near clusters of variable host specificity and interaction genes, was only found in the OtV-type 2b virus genomes (Fig. 3). In eukaryotes, the Rad50 protein is associated with the Mre11 protein (the bacterial homolog of the SbcD/SbcC system; Pandey et al. 2018), which is involved in repairing DNA double-strand breaks (Lammens et al. 2011, Storvik and Foster 2011). The structure of this protein in OtV-type 2b viruses was predicted with low confidence (pTM = 0.29) to fold as a long alpha-helix coiled-coil domain and two mixed beta-strands in the N- and C-terminal. Foldseek search revealed no obvious function and did not detect any similarity with Mre11. Tentative pairwise alignment with, e.g. 5F3W and 4YKE Mre11 experimental structures failed as well. However, due to the low homology of Rad50 protein with other organisms and the lack of homology for an Mre11-like domain, it remains challenging to draw any conclusions about the function of the gene and its association with the large structural variations specific to OtV-type 2b.

To identify molecular signatures associated with evolutionary processes in host–virus interactions, the ratios (ω) of nonsynonymous (Ka) and synonymous (Ks) substitution rates were estimated in each OtV-type across different alignments for genes in the HVR with >80% nucleotide sequence identity (Fig. 3; Supplementary Table 6). A total of seven distinct groups of homologous genes (orthogroups) could be tested. Of these seven orthogroups, five showed a low ratio across five different models tested. This concerns a capsid protein central to HVR for both OtV-type 1 and OtV-type 2a groups (an average of $\omega = 0.02$ and P-value = 2e-105), a gene coding for a rad50 protein in the OtV-type 2b group (an average of $\omega = 0.21$ and a P-value = 3e-68) and one of the cell wall anchor surface family proteins (FhaB) in the OtV-type 2a group (an average of $\omega = 0.1$ and a P-value = 3e-16). Ka /Ks ratios below one are indicative of purifying (negative) selection, implying that these proteins are functionally constrained and likely play critical roles in the viral infection cycle. Interestingly, two orthogroups, both coding for putative FhaB proteins, showed high Ka /Ks ratios in the OtV-type 1 and the OtV-type 2a groups. While for OtV-type 1, Ka /Ks ratios vary between models, the NG model suggests significant positive selection, with an average of $\omega = 1.42$ and a P-value = .008. For OtV-type 2a, Ka /Ks ratios were consistently >1 across all models, with highly significant P-values (average of $\omega = 1.3$ and a P-value = 3e-155), indicating strong diversifying (positive) selection. These results suggest that these proteins may undergo rapid adaptive evolution, likely driven by interactions with their hosts, which could in turn facilitate host range expansion or enable escape from host defenses.

To further investigate the putative functions of genes associated with the HVR, 124 protein sequences, from all genomes in the OtV-type 2b, the OtV19-O (OtV-type 1), and two genomes from OtV-type 2a (OtV09-582 and OtV5), were submitted to AlphaFold3 for the computational prediction of their 3D structures (Abramson et al. 2024). The length of the sequences ranged between 58 and 2188 amino acids. All targeted proteins yielded predictions with overall accuracy reported by template modelling scores (pTM) ranging from 0.23 to 0.93. Confident high-quality predictions were made for 37 protein models ($pTM \geq 0.80$), 21 had intermediate confidence ($0.60 \leq pTM \geq 0.80$) while 66 models were not sufficiently reliable to obtain structural predictions ($0.60 \leq pTM$). We chose 58 of the 124 models for submission to a protein structural similarity search with Foldseek (van Kempen et al. 2024). Principal hits were searched in the structural databases AlphaFold/Proteome, AlphaFold/Swiss-Prot, AlphaFold/UniProt50, and PDB100, confirming the presence of peptidase S74, ABC1 domain-containing protein, autotransporters, glycosyl- or carbohydrate-related proteins, and phage-tail proteins. Detailed analysis of 13 FhaB common to the HVR revealed elongated β folds (Fig. 3b). The viral FhaB homologs (OtV06-12-00065, OtV09-565-00065, OtV19-O-00074, OtV09–582-00074, and OtV5–070) were predicted to form a right-handed β-helix structure consisting of 42–63 strands, with three faces each made up of parallel β-strands. Overall, they form a β-3-solenoid (CATH ID: 2.160.20). The two homologs in OtV09-582 and the OtV5 (i.e. OtV09-582-00075 and OtV5-071) were predicted to form an elongated 30–48-strand single parallel β-sheet folding as a right-handed helical solenoid and respectively spanned 21.2 and 13.6 nm in their longest dimension. Both fibrillar architectures are therefore likely to generate extra-virion projections and facilitate intermolecular recognition.

OtV-type 2b viruses display the broadest host range

A cross-infectivity assay was carried out on all viruses studied in this work against a panel of nine *O. tauri* strains by spotting viruses onto hosts grown on soft agarose plates. Note that both OtV19-T1 and OtV19-T2 viruses originated from the same lysate (OtV19-T) and, therefore, could not be studied for host range separately.

Three different viral infection patterns were observed: (i) no lysis, which was characterized by the absence of plaques, (ii) strong lysis, which was defined by large and well-rounded plaques, and (iii) lower lysis, which gave smaller and more turbid plaques (Fig. 4a). As expected, only *Ostreococcus* strains were susceptible to infection by OtVs (Fig. 4b). The two *Micromonas* and *Bathycoccus* strains showed no lysis, indicating a specificity of the genus *Ostreococcus* of these viruses. All lysates infected at least one of the *O. tauri* strains tested, while OtV-Sylt2-5 and OtV09-573 were also able to infect *O. mediterraneus* strain RCC789. Our analysis revealed that the *O. tauri*-OtV cross-infection assay exhibited a 'nested' or hierarchical structure. In this structure, the viral host range was on a continuum from specialized viruses infecting a narrow range of host strains to generalist viruses infecting a broader range of hosts. The OtV5, OtV06-1, and OtV19-O viruses displayed the narrowest host range (i.e. specialist), infecting only the most susceptible strain, *O. tauri* RCC4221. In contrast, the OtV09-578, OtV06-12, and OtV09-565 viruses, which were associated with the OtV-type 2b group and whose hypervariable region was characterized, were viruses with the broadest host range (i.e. generalists), infecting all the strains tested (Fig. 4b).

Interestingly, 67% of viruses (8 out of 12 viruses) showed changes in infection pattern in comparison to the previous analysis (Clerissi et al. 2012). The switch from noninfectivity to infectivity was the most reported phenotypic change (15 out of 20—75%), rather than the shift from infectivity to noninfectivity (5 out of 20—25%) (Fig. 4b). In addition, those changes were mostly observed for the two most generalist viruses (i.e. OtV06-12 and OtV09-570) and for one of the host strains most susceptible to infection (*O. tauri* RCC1117 strain). Our analysis revealed a statistically significant, although weak, positive correlation between the host range and the HVR length (p=.0051, $r = 0.62$, $R^2 = 0.38$) (Fig. 4c), implicating these gene expansions as the genetic determinants of increased host range. Nonetheless, two OtV strains stood out as clear outliers in terms of this association,

Downloaded from https://academic.oup.com/ve/article/12/1/veaf096/8472608 by guest on 18 February 2026

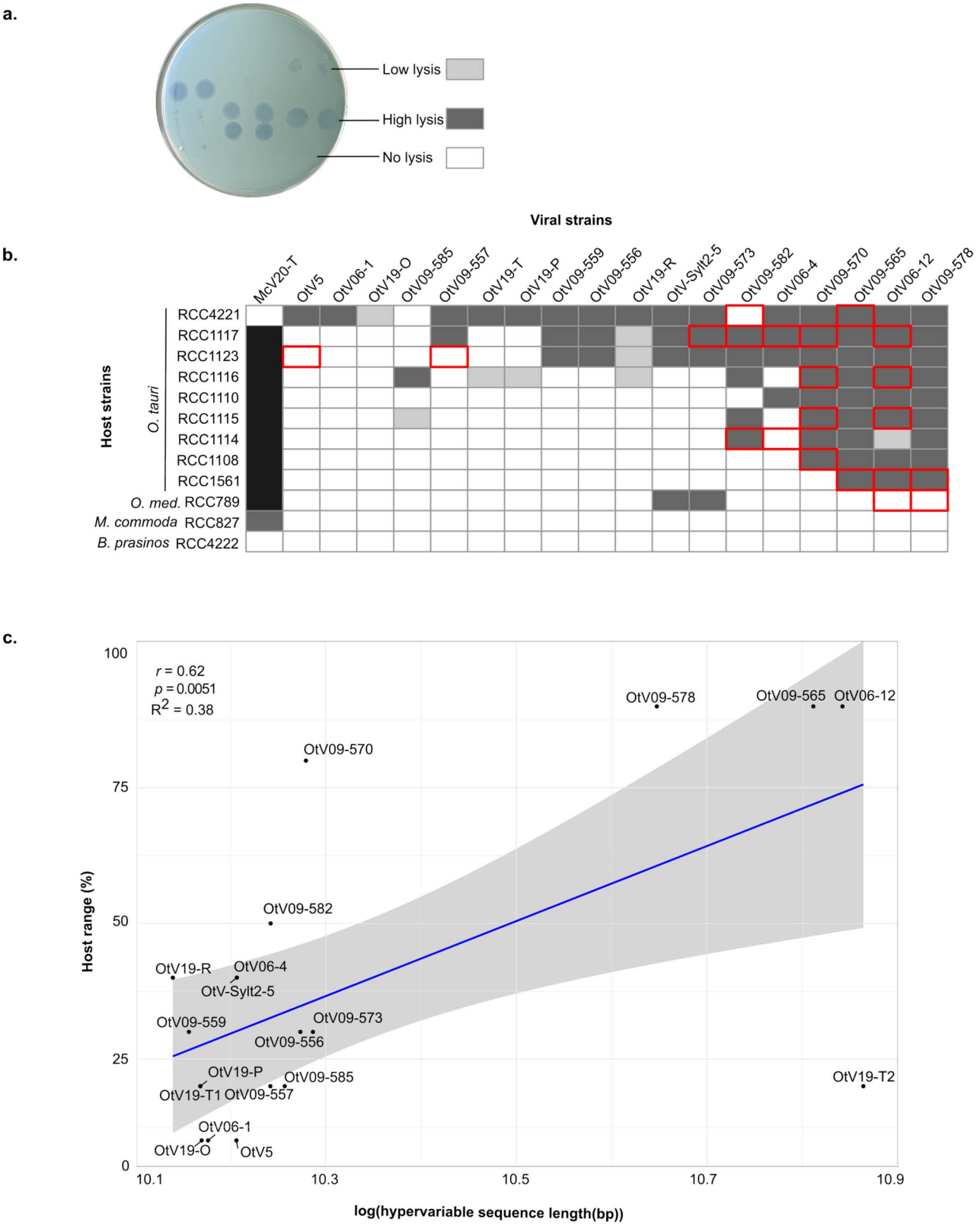


Figure 4. Host–virus infection patterns. (a) Example of plaque assays for different viral infections showing low, high, and no lysis for a given phytoplankton host strain. (b) Cross-infectivity assays of OtVs against a panel of *Ostreococcus* sp. strains (*O. tauri*, *O. mediterraneus*) and two representative species of the most closely related genera within the Mamiellophyceae class (*M. commoda* and *Bathycoccus prasinos*). No lysis indicates that no plaques were observed. Low lysis indicates that the lysis plaques were smaller or more turbid, while high lysis indicates that large plaques were observed three days after infection. Note that phenotypic changes observed compared to the data of Clerissi et al. (2012) were framed around the boxes. The host range of McV-20 T was only tested on the strains *M. commoda* RCC827, *O. tauri* RCC4221, and *B. prasinos* RCC4222. (c) Linear correlation between the host range and the hypervariable sequence length of OtVs. The host range is represented in percentage, i.e. the number of successful lysis divided by the total number of *Ostreococcus* strains tested in the experiment (i.e. 10 strains). The x-axis is log-transformed for a clearer visual representation of the data. Note, log transformation slightly reduced residual variance and model error but did not substantially improve the overall fit. *R*, Pearson correlation coefficient; *P*, *P*-value; and R^2, coefficient of determination.

Downloaded from https://academic.oup.com/ve/article/12/1/veaf096/8472608 by guest on 18 February 2026

namely, OtV09-570, which had no obvious expansion in HVR size but an apparently broad host range, and OtV19-T2, which had a large HVR expansion but a narrow host range. As the variability in host range over time particularly affected OtV09-570, this suggests that this strain may be given to rapid variation in host range with time or be phenotypically variable. This variability in host range clearly complicated a direct association between genotype and host range.

The *O. tauri*–prasinovirus dynamics are highly variable between strains

To compare the dynamics of infection between viral strains of the same phylogenetic clade with the aim to better link viral genetic features to infection traits, four *O. tauri* strains (RCC4221, RCC1123, RCC1116, and RCC1108) with a range of patterns of susceptibility to OtVs (Fig. 4) were challenged in liquid assay with the sixteen OtVs of type 2 (Fig. 5). Overall, the infection dynamics differed between the different *O. tauri* strain populations showing strain-specific responses to infection by OtV strains. As expected, the *O. tauri* RCC4221 was the most susceptible strain to all the viruses tested, showing lysis in response to the same virus strains as in the cross-infection spot-based assay (Fig. 4). In addition, the lysis dynamics of *O. tauri* RCC4221 in response to infection by OtV strains occurred along a continuum in terms of time to lysis, speed of lysis, and mortality. By contrast, *O. tauri* RCC1108, which was the least susceptible strain (Fig. 4), showed strong lysis in response to two OtVs (OtV09-565 and OtV09-578) in liquid culture (Fig. 5a and Supplementary Fig. 9). However, RCC1108 was not lysed by two additional viruses, OtV09-570 and OtV06-12, as in the spot assay (Fig. 4). Similarly, RCC1116 was lysed in liquid culture by four viruses (i.e. OtV09-565, OtV09-578, OtV09-582, OtV09-585) but was not visibly lysed by an additional four viruses (i.e. OtV06-12, OtV09-570, OtV19-T, OtV19-R) that produced plaques in Fig. 4. Intriguingly, RCC1123 showed the inverse case with lysis occurring from infection by OtV09-557 in liquid culture (Fig. 5a and Supplementary Fig. 9) but with no plaques in the spot assay (Fig. 4). Host-strain-specific responses were evident in the comparison of the lysis dynamics of the most generalist virus strains, OtV09-565 and OtV09-578, which showed the degree of mortality varied with each host strain. For example, RCC1116 lysed relatively slowly in response to infection by these two viruses, whereas it showed a higher degree of mortality to strains OtV09-582 and OtV09-585. Altogether, this revealed that successful lytic viral infection can indeed depend on the growth conditions, in this case, if the growth medium was semisolid or liquid, indicating a factor strongly influencing the variability in host range. The variation in host range between the two assays was most pronounced for the strain OtV09-570, which lysed only RCC4221 instead of all four tested strains as expected from the plaque assay, again indicating it as the most variable in host range.

We measured viral particle concentration at the end of the 15-day time course and observed that the host lysis dynamics were not well associated with our proxy of viral production (Fig. 5b). Clear virus production could only be associated with lysis of the most susceptible strain RCC4221, and with strong lysis by the most generalist strains OtV09-565 and OtV09-578, which allowed us to infer these host–virus interactions resulted from productive infections. However, there were multiple apparent cases of virus production that were not associated with cell lysis. The clearest example was the *O. tauri* RCC1108 strain, where the proportional change over 15 days in OtV06-4 viral particle concentration was five, like the OtV09-565 virus, but with no host mortality. Another notable example is the *O. tauri* RCC1123 strain, in which the OtV19-T virus showed a proportional change of viral concentration of 2.5, while no host lysis was detected.

Prasinoviruses show distinct morphologies

Morphological investigations using TEM were carried out on the new viruses isolated in this study (i.e. OtV19-P, OtV19-O, OtV19-T, OtV19-R and OtV-Sylt2-5), as well as on the viruses associated with OtV-type 2b (i.e. OtV06-12, OtV09-578, and OtV09-565), in comparison with the OtV5 virus, previously characterized (Derelle et al. 2008).

Overall, the OtVs shared a common morphology; they produced non-enveloped virions with an icosahedral capsid having an averaged diameter of 140 ± 8 nm (Fig. 6a). Furthermore, notable phenotypes were observed for the two viruses OtV09-565 and OtV19-T. The OtV19-T lysate, in which two distinct genotypes were characterized in this study, consisted of two morphotypes (Fig. 6a; Supplementary Fig. 10a). The first morphotype was comparable to that observed for the majority of OtVs, i.e. non-enveloped with an icosahedral capsid, with a diameter of 139 ± 10 nm. By contrast, the second morphotype appeared 'squashed', with the flattening of a vertex and the widening along the diameter (148 ± 8 nm). Such changes might be the result of genetic and/or structural constraints that affected capsid protein arrangement, especially under specific environmental conditions. It is tempting to speculate that the two morphologies of OtV19-T corresponded to the two different genotypes. Finally, a striking new morphological feature was observed in OtV09-565. This virus produced virions with an icosahedral capsid (averaged diameter of 140 ± 9 nm) to which was connected an elongated and flexible structure of 154 ± 46 nm and 21 ± 5 nm in length and width, respectively (Fig. 6a and b). This structure appeared to be tail-like and superficially like those of viruses in the *Caudovirales*. It emerged from one vertex, but no other structures, such as spikes or a base plate, were observed. On the other hand, the lysate consisted of a mixture of tailed and non-tailed virions, with a slightly higher proportion of the tailed particles (Fig. 6c). Free tails were also observed next to nontailed particles, indicating the lability of this structure (Supplementary Fig. 10b). Moreover, no significant difference in capsid size was detected between the two types of virions, supporting the hypothesis of a single viral population (Fig. 6b).

Finally, to further investigate the biological function and potential role of the tail-like structure of OtV09-565 during infection, thin sections of both uninfected and infected algal cultures were examined using TEM. For uninfected conditions, images revealed healthy cells, as expected, with intact organelles such as chloroplast, nucleus, mitochondrion, cytoplasm, and starch grain (Supplementary Fig. 11). In infected cells, a viral particle was observed near a cell 5 min after infection. While a thin structure connecting the capsid and the cell surface was observed during the attachment phase (at 30 min), no tail-like appendage associated to the capsid could be identified in this case. Intracellular virions were first observed in the cytoplasm at 4 h postinfection (hpi). By 12 hpi, the cell became packed with viral particles, ready for lysis to release the newly formed virions. Finally, at 72 hpi, the cells are completely lysed with viral particles in suspension in the medium (Supplementary Fig. 11). The tail-like structure was not observed in any stage during assembly or release.

Discussion

In this study, we sought to expand our knowledge about the diversity of the *Prasinovirus* genus by isolating new viruses from

Downloaded from https://academic.oup.com/ve/article/12/1/veaf096/8472608 by guest on 18 February 2026

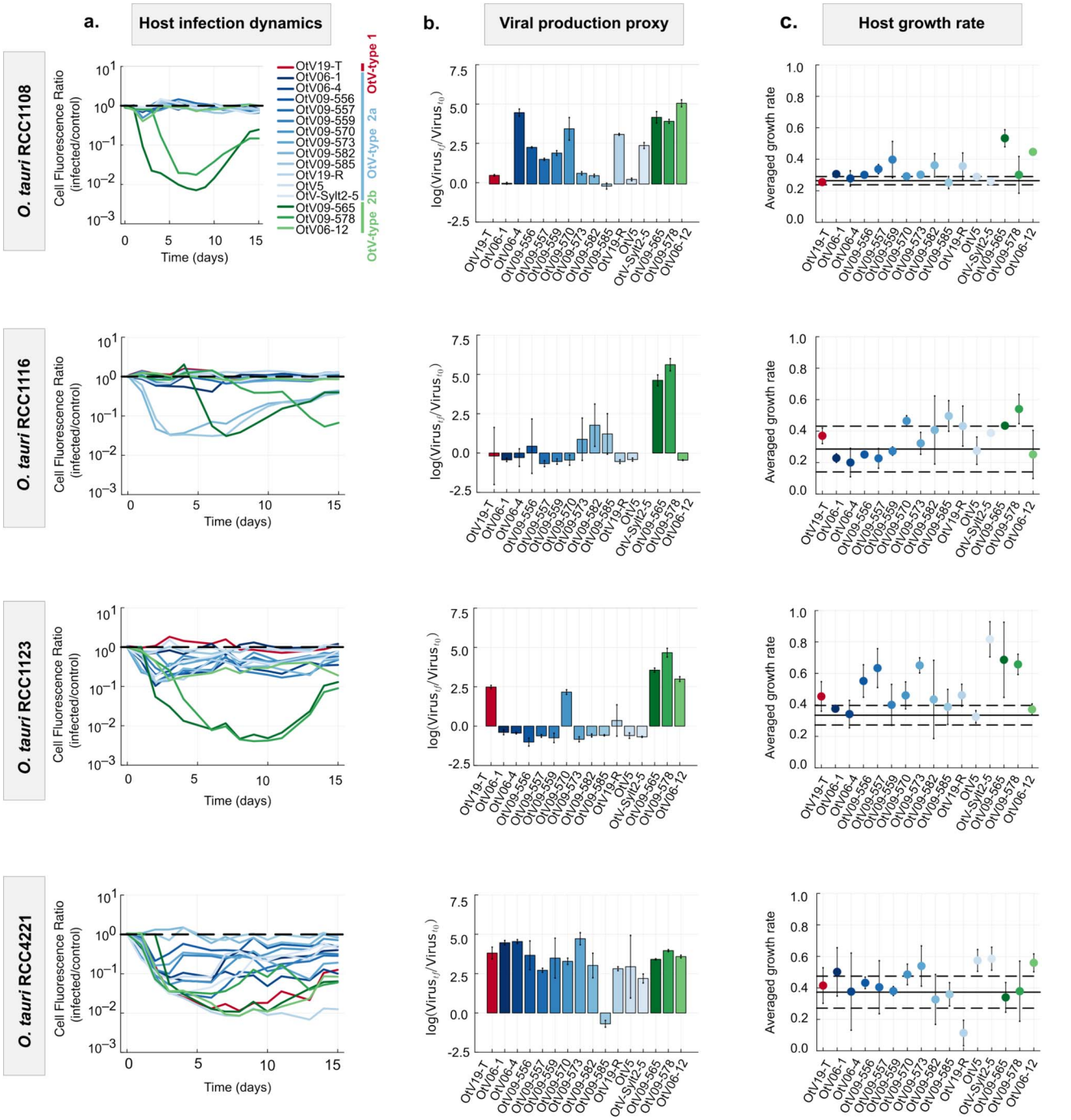
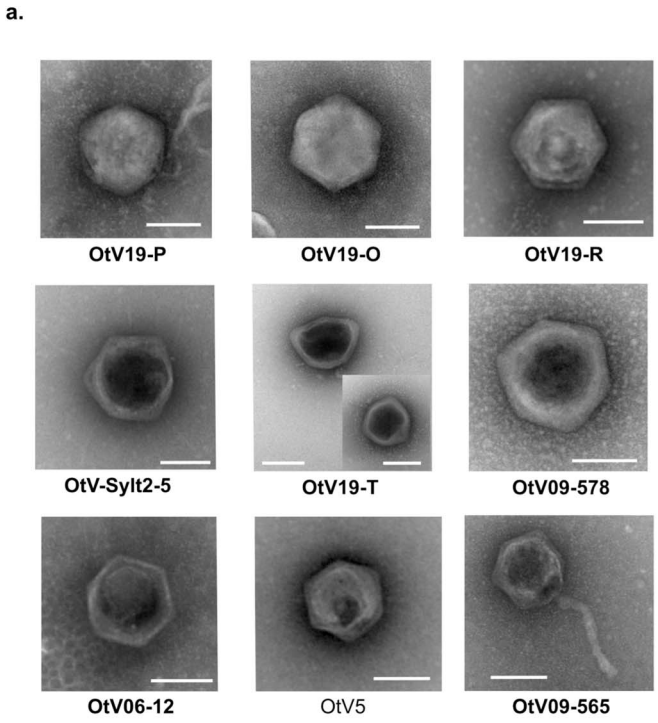


Figure 5. Infection dynamics of *O. tauri* strains and the OtVs. The four *O. tauri* strains tested (RCC1108, RCC1116, RCC1108, and RCC4221) were sorted in rows, and for each host, the following parameters were measured: (a) averaged host dynamics ($n = 3$) plotted as the cell fluorescence ratio in infected versus noninfected (control) cultures. The black dashed line corresponds to the baseline cell density of the control. Colored lines below the dashed line indicate infected cultures with a decrease in cell density relative to the uninfected controls. (b) Proxy of virus production calculated as the natural log-transformed ratio of virus concentration at the final time versus inoculation time. (c) Averaged population growth rate (in days) of the cells in the recovery phase. Error bars represent the standard deviation of the mean ($n = 3$). Solid and dashed black lines represent the averaged growth rate and standard deviations, respectively, in the control culture. The growth rate has been estimated as the slope of the linear regression of the log-transformed cell concentration during the exponential re-growth in the recovery phase.

distant locations around the world. The sequencing of 18 new complete OtV genomes has shed light on the diversification and evolution of these viruses and the genetic signatures associated with their host range. To date, prasinovirus genomes have been observed with a high degree of conservation of the order of homologous genes (Moreau et al. 2010). In this work, we describe an organization of OtV genomes modularly defined with both synthetic and nonsyntenic regions. A similar pattern was observed in *Ostreococcus lucimarinus* virus (OlV) genomes, where a central and large DNA fragment was inverted, distinguishing two subgroups of OlV (Derelle et al. 2015). Here, we defined three distinct new OtV clades, classified as OtV-type 1, OtV-type 2a,

Downloaded from https://academic.oup.com/ve/article/12/1/veaf096/8472608 by guest on 18 February 2026



Virus	OtV-type	Dimensions
OtV19-P	1	134 ± 7 nm
OtV19-O	1	135 ± 8 nm
OtV19-T	1/2b	148 ± 8 nm
		139 ± 10 nm
OtV5	2a	149 ± 10 nm
OtV-Sylt2-5	2a	143 ± 10 nm
OtV19-R	2a	142 ± 5 nm
OtV09-578	2b	144 ± 7 nm
OtV09-565	2b	140 ± 9 nm
OtV06-12	2b	133 ± 10 nm

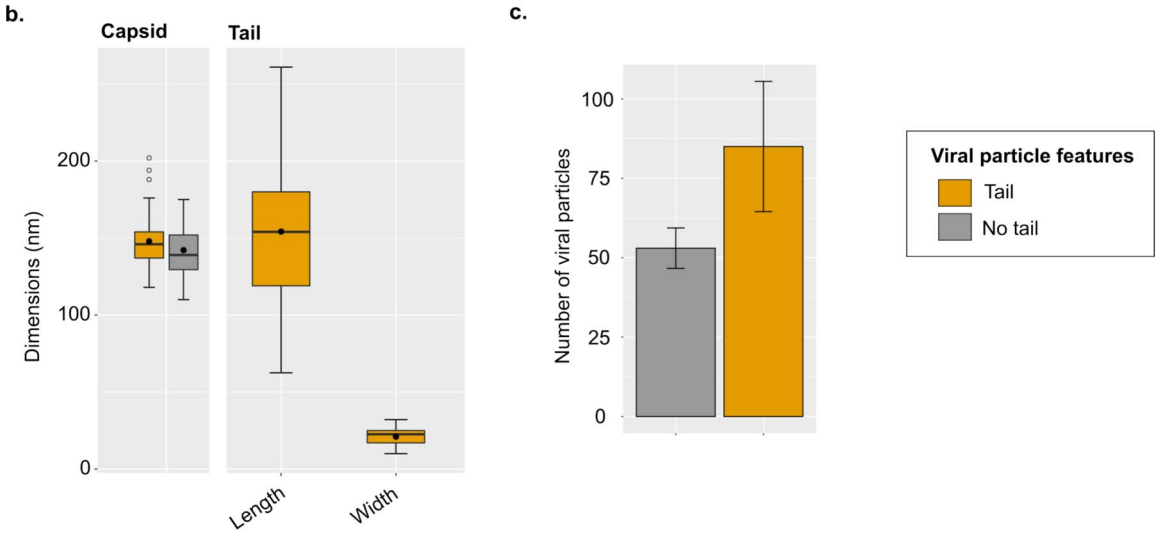


Figure 6. Morphological characterization of *O. tauri* viruses. (a) Transmission electron micrograph of OtV particles. The viruses isolated from the Pacific Ocean (OtV19-O, OtV19-P, OtV19-T, OtV19-R) as well as the North Sea virus (OtV-Sylt2-5) were compared to the Mediterranean viruses associated with OtV-type 2b than OtV5 (OtV-type 1). Viruses newly characterized in this study are bolded. The scale bar corresponds to 100 nm. The dimensions are shown as the average and standard deviations of the capsid dimensions (width). (b) The capsid size of the tailed virion was compared to the nontailed one, and the length and width of the tailed viral particles were reported. (c) Bar plot showing the number of tailed-virion or nontailed in a lysate obtained 3 days post-infection.

and OtV-type 2b, which showed distinct evolutionary relationships. Notably, OtV-type 1, relatively divergent from other OtVs, forms a subclade within the *Micromonas* viruses clade. Furthermore, ~60% of the OtV-type 1 clade-specific proteins were homologues in the genomes of *Micromonas* virus, including the new McV20-T virus, which were absent from all other *Ostreococcus* viruses. Our results were consistent with the previous work of Thomy et al. using a targeted enrichment approach in the South China Sea (Thomy et al. 2024). The authors identified a new viral clade, termed clade III, consisting of a set of *Micromonas* and *Ostreococcus* viruses, including the previously sequenced OtV6 genome. This clade branches into the *Micromonas* virus clade. Here, our work further supports the idea of host switching between genera and the hypothesis of host range expansion, although these viruses failed to infect the *Micromonas commoda* RCC827 strain. We also suggest the possibility that these viruses evolved from a common ancestor infecting the hosts *Micromonas* and *Ostreococcus* or an intermediate lineage. A recent study identified an isolated *Micromonas*-infecting virus that diverges from other *Micromonas* viruses and instead forms a basal branch relative

Downloaded from https://academic.oup.com/ve/article/12/1/veaf096/8472608 by guest on 18 February 2026

to the clade of *Bathycoccus*-infecting viruses. This pattern suggests that *Micromonas*-infecting viruses may represent an earlier-branching lineage within the prasinoviruses (Bedi de Silva et al. 2025). Overall, these results raise several questions about the evolution and ecology of prasinoviruses. Could these viruses expand their host range by infecting the same host through recombination events and horizontal gene transfer? Although no evidence of homologous recombination events was found in the OtV genomes in this study, we were able to describe the horizontal transfer of a gene encoding the 18 kDa mitochondrial protein from *Ostreococcus* and *Micromonas* strains to OtV-type 1 viruses and some *Micromonas* viruses. This result suggests that the acquisition of this gene either occurred independently in both lineages or that a common ancestor acquired it from a host before diverging into two separate lineages. Although the exact role of the 18 kDa mitochondrial protein in algae is not yet fully understood, in animals, this receptor is recognized as crucial for cellular respiration, steroid hormone production, cell death, and immune response (Papadopoulos et al. 2006). Hence, it is likely that the 18 kDa protein plays a key role in host metabolism, potentially benefiting viral infection. This strongly supports the hypothesis that OtV-type 1 have adapted both to their hosts and to the environmental conditions. In addition, most of the clade-specific genes, including the 18 kDa protein, were found in a cluster, appearing in genomic islands or, as described in this study, VSRs.

The adaptability of viruses to extend their host range is driven by genetic changes such as mutations, recombinations, and rearrangements mainly targeting genes involved in attachment to a receptor at the host cell surface (Ferris et al. 2007, Zhao et al. 2019). In bacteriophages, such mutations have been found in host recognition modules encoding tail fibres, chaperones, and baseplates (Hashemolhosseini et al. 1994, Tétart et al. 1996, Kizziah et al. 2020, Gonzalez-Serrano et al. 2023). In contrast, the genetic basis of host-range evolution in eukaryotic dsDNA viruses is poorly understood. In this study, we highlighted an HVR in the OtV genomes that is characterized by numerous mutations in genes encoding surface proteins and/or receptor-binding domains involved in viral recognition and attachment to the host cell. Furthermore, this high genetic plasticity was mainly detected in OtV-type 2b, the group of viruses with the broadest host range. We propose that this region acts as a hotspot for genomic recombination and diversification. This process is driven by strong coevolutionary arms-race dynamics, in which viruses continuously adapt to overcome host defences and hosts evolve to evade viral infection. Such dynamics parallel those extensively documented in bacteriophage–bacteria systems, where host recognition genes undergo rapid diversification (Comeau et al. 2007, Labrie et al. 2010).

Additionally, our data revealed that viruses from geographically distinct locations can infect identical host strains. One possible explanation involves an alternative infection pathway that enables these viruses to target the same host strain without necessarily broadening their host range. Notably, a specific genomic region identified in this study as VSR1 was exclusively shared between OtV-type 1 and OtV-type 2a, two virus groups originating from different geographical regions. This region encodes genes involved in fatty-acid, amino-acid and, secondary metabolisms as well as carbohydrate metabolism including glycosyltransferases. In contrast, only glycosyltransferases with low sequence homology with other groups were found in OtV-type 2b viruses from this same region. The carbohydrate biosynthetic enzymes, including glycosyltransferases, have been documented in giant viruses (Speciale et al. 2022). Glycosylation-related genes encoded by viruses allow them to become partially or completely host-independent by modifying their own glycoproteins. This feature was thought to be a viral strategy for evading cellular immunity by mimicking host glycans. In addition, the glycosylation of capsid proteins may also influence host cell attachment and entry, playing a potential role in host specificity. To date, glycosylation of the chlorovirus capsid protein has been the most widely studied of the giant viruses (Wang et al. 1993; Graves et al. 2001; Nandhagopal et al. 2002; Van Etten et al. 2010; Xiang et al. 2010). However, although the exact mechanism of glycosylation in prasinoviruses is still poorly understood, we propose that this region might be an alternative pathway encoding the glycosylation of the viral capsid in determining host specificity.

Furthermore, our analysis revealed variability in the host range, which particularly affected OtV09-570. This suggests that this virus may undergo rapid changes in host range over time or exhibit phenotypic variability. This variability in host range clearly complicated a direct association between genotype and host range. Given this pattern of HVR variability and variability in host range, we hypothesized that the genetic determinants of the host range likely involved a complex mechanism of multiple genetic features interacting specifically with the host strain genetics. Moreover, given the variation over time in our spot assay, host range may be evolving rapidly over time, or it may be a variable trait when measured with this assay. Also, host range may be sensitive to variations in other, yet unidentified factors, such as variations in abiotic factors. Beyond the host range, analyses of infection dynamics have revealed substantial temporal variability. Initially, the lack of correspondence between lysis and viral production was due to a limitation of the experimental setup, in which we could only measure virus concentration at the end of the experiment. This meant that we could not observe virus dynamics, such as virus decay, during the 15-day time course. This phenomenon could also be explained by (i) heterogeneity in the host populations, such as virus production from a subpopulation of susceptible cells in a majority virus-resistant population, or (ii) a chronic infection in which viral particles are produced by a budding mechanism without cell lysis. The former case was observed in resistant populations of *O. tauri* and *O. mediterraneus* (Yau et al. 2016, 2020), while the latter hypothesis was previously proposed by Thomas et al. for the *O. tauri* strain and the OtV5 virus as a mechanism of viral resistance (Thomas et al. 2011).

The acquisition of the resistance, or cell recovery, is defined as the phase in which the concentration of viable cells re-increases after a lysis phase. This phenomenon has been previously described in Mamiellophyceae (Thomas et al. 2011, Yau et al. 2018). In this work, we observed that resistance occurred in all cross-infections (30 crosses) except for two (i.e. OtV19-R on RCC4221, OtV09-578 on RCC1116) in the 15-day time frame of the experiment (Fig. 5c and Supplementary Fig. 9). This indicated that development of resistance was a highly consistent trait irrespective of the host–virus strain interactions. In addition, all recovered cultures showed a population growth rate equal to or higher than that of the uninfected culture (control) (Fig. 5c), suggesting that the development of resistance had no detectable 'cost of resistance' trade-off (Bohannan & Lenski 2000); Bohannan et al. 2002) visible in the population growth rate. Overall, these findings showed that the *O. tauri*-prasinovirus system has a high variability in the infection dynamics, which was specific to the host and virus strain combination, and the host recovery response was a highly consistent trait in the *O. tauri* strains tested.

Genome analyses identified putative tail components in several OtV genomes, including OtV-type 1 viruses OtV09-559, OtV09-565, OtV09-578, and OtV06-12. These components encompassed

Downloaded from https://academic.oup.com/ve/article/12/1/veaf096/8472608 by guest on 18 February 2026

the phage tail fiber protein and the phage tail assembly chaperone protein. This genetic architecture, in which the genes of tail components are clustered together within the genome, resembles that described in tailed phages of the order *Caudovirales* (Fokine and Rossmann 2014). Notably, the hypervariable region—comprising host recognition and attachment genes—exhibits rapid adaptation, likely to accommodate new hosts or evade host resistance. Such evolutionary dynamics are well documented in tailed phages (Comeau et al. 2007, Paterson et al. 2010, de Leeuw et al. 2020, Holtzman et al. 2020). In our study, TEM images revealed a tail-like structure associated with the capsid in the virus OtV09-565. Thus, OtV09-565 represents the first reported *Ostreococcus*-infecting virus with a tail-like structure. A comparable structure, including a tail-like appendage and thin fibres for host attachment, has been reported in the *Micromonas* virus MpVN1 (Zingone et al. 2006). However, thin-section TEM of OtV09-565-infected cells showed no visible tails during intracellular capsid assembly stages, leading to the tentative conclusion that tails are not attached at this stage. How and when the tail structure is formed remains an open question requiring further study. We speculate that it may occur during release, or the tail could be induced extracellularly, such as a structure ejected from the viral core. Establishing a direct correlation between the genetic repertoire and the phenotype remains challenging. While several other viruses encode putative tail components in their genomes, a tail-like structure has only been observed in OtV09-565. This difference may be due to the lability of the tail, which could limit its detection in other viruses.

By integrating computational and experimental approaches, our study offers comprehensive insights into the genetic diversity of OtVs and, for the first time, describes a form of viral plasticity potentially driven by antagonistic coevolution with host organisms. In addition, we report novel morphological features that may play a key role in host–virus interactions. Overall, these data provide a better understanding of how marine viruses that infect eukaryotes adapt and evolve in response to changing environmental conditions and pressures from the host immune system in the ocean.

Acknowledgements

We would like to thank Morgan Gaïa, Vladimir Daric, and Hélène Mayer of the BSBII, Banyuls Bioinformatic Service; genotoul bioinformatics platform Toulouse Occitanie (Bioinfo Genotoul, https://doi.org/10.15454/1.5572369328961167E12) for providing help and computing and storage resources and Christophe Salmeron and David Pecqueur from the SU/CNRS BioPIC Imaging and Cytometry platform of Oceanographic Observatory of Banyuls-sur-Mer, whose French state funds are managed by the ANR within the Investments of the Future program under reference ANR-10-INBS-02.

Supplementary data

Supplementary data are available at *VEVOLU Journal* online.

Conflict of interest: None declared.

Funding

ANR ALGALVIRUS (ANR-17-CE02-0012), Emergence 2023–2025 Sorbonne Université, PRAMA.

Data availability

The genome sequences and annotations are available on Genbank with the following accession numbers: McV20-T, PQ442261; OtV06-1, PQ442262; OtV06-12, PQ442263; OtV06-4, PQ442264; OtV09-556, PQ442265; OtV09-557, PQ442266; OtV09-559, PQ442267; OtV09-565, PQ442268; OtV09-570, PQ442269; OtV09-573, PQ442270; OtV09-578, PQ442271; OtV09-582, PQ442272; OtV09-585, PQ442273; OtV19-O, PQ442274; OtV19-P, PQ442275; OtV19-R, PQ442276; OtV19-T1, PQ442277; OtV19-T2, PQ442278; OtV-Sylt2-5, PQ442279.

The raw sequencing data have been submitted to Genbank under Bioproject number PRJNA1345089.

The complete list of AlphaFold3 models is available for download: (https://dropsu.sorbonne-universite.fr/s/8RREeAoBoDastwp).

References

Abramson J, Adler J, Dunger J *et al.* Accurate structure prediction of biomolecular interactions with AlphaFold 3. *Nature* 2024;**630**:493–500. https://doi.org/10.1038/s41586-024-07487-w

Agrawal AF, Lively CM. Modelling infection as a two-step process combining gene-for-gene and matching-allele genetics. *Proc R Soc Lond Ser B Biol Sci* 2003;**270**:323–34. https://doi.org/10.1098/rspb.2002.2193

Andrews S. *FastQC: A Quality Control Tool for High Throughput Sequence Data*. Babraham Bioinformatics, Babraham Institute, Cambridge, UK. 2010.

Avrani S, Wurtzel O, Sharon I *et al.* Genomic island variability facilitates Prochlorococcus–virus coexistence. *Nature* 2011;**474**:604–8. https://doi.org/10.1038/nature10172

Aylward FO, Moniruzzaman M, Ha AD *et al.* A phylogenomic framework for charting the diversity and evolution of giant viruses. *PLoS Biol* 2021;**19**:e3001430. https://doi.org/10.1371/journal.pbio.3001430

Azam AH, Kondo K, Chihara K *et al.* Evasion of antiviral bacterial immunity by phage tRNAs. *Nat Commun* 2024;**15**:9586. https://doi.org/10.1038/s41467-024-53789-y

Bachy C, Charlesworth CJ, Chan AM *et al.* Transcriptional responses of the marine green alga Micromonas pusilla and an infecting prasinovirus under different phosphate conditions. *Environ Microbiol* 2018;**20**:2898–912. https://doi.org/10.1111/1462-2920.14273

Bachy C, Yung CCM, Needham DM *et al.* Viruses infecting a warm water picoeukaryote shed light on spatial co-occurrence dynamics of marine viruses and their hosts. *ISME J* 2021;1–19. https://doi.org/10.1038/s41396-021-00989-9

Bankevich A, Nurk S, Antipov D *et al.* SPAdes: A new genome assembly algorithm and its applications to single-cell sequencing. *J Comput Biol* 2012;**19**:455–77. https://doi.org/10.1089/cmb.2012.0021

Baudoux A-C, Lebredonchel H, Dehmer H *et al.* Interplay between the genetic clades of micromonas and their viruses in the western English Channel. *Environ Microbiol Rep* 2015;**7**:765–73. https://doi.org/10.1111/1758-2229.12309

Bedi de Silva A, Polson SW, Schvarcz CR *et al.* Genomic diversity and global distribution of four new prasinoviruses from the tropical North Pacific. *Microbiol Spectr* 2025;**13**:e02583–24. https://doi.org/10.1128/spectrum.02583-24

Bellec L, Grimsley N, Derelle E *et al.* Abundance, spatial distribution and genetic diversity of Ostreococcus tauri viruses in two different environments. *Environ Microbiol Rep* 2010;**2**:313–21. https://doi.org/10.1111/j.1758-2229.2010.00138.x

Downloaded from https://academic.oup.com/ve/article/12/1/veaf096/8472608 by guest on 18 February 2026

Bellec L, Clerissi C, Edern R *et al.* Cophylogenetic interactions between marine viruses and eukaryotic picophytoplankton. *BMC Evol Biol* 2014;**14**:59. https://doi.org/10.1186/1471-2148-14-59

Bidle KD. Programmed cell death in unicellular phytoplankton. *Curr Biol* 2016;**26**:R594–607. https://doi.org/10.1016/j.cub.2016.05.056

Bohannan BJM, Lenski RE. Linking genetic change to community evolution: Insights from studies of bacteria and bacteriophage. *Ecol Lett* 2000;**3**:362–77. https://doi.org/10.1046/j.1461-0248.2000.00161.x

Bohannan BJM, Kerr B, Jessup CM *et al.* Trade-offs and coexistence in microbial microcosms. *Antonie Van Leeuwenhoek* 2002;**81**:107–15. https://doi.org/10.1023/A:1020585711378

Brussaard CPD. Optimization of procedures for counting viruses by flow cytometry. *Appl Environ Microbiol* 2004;**70**:1506–13. https://doi.org/10.1128/AEM.70.3.1506-1513.2004

Brussaard CPD, Baudoux A-C, Bratbak G *et al.* Phaeocystis and its interaction with viruses. *Biogeochemistry* 2007;**83**:201–15.

Chan PP, Lowe TM. tRNAscan-SE: Searching for tRNA genes in genomic sequences. *Methods Mol Biol* 2019;**1962**:1–14. https://doi.org/10.1007/978-1-4939-9173-0_1

Chen H, Zhang W, Li X *et al.* The genome of a prasinoviruses-related freshwater virus reveals unusual diversity of phycodnaviruses. *BMC Genomics* 2018;**19**:49. https://doi.org/10.1186/s12864-018-4432-4

Chrétiennot-Dinet M-J, Courties C, Vaquer A *et al.* A new marine picoeucaryote: Ostreococcus tauri gen. Et sp. nov. (Chlorophyta, Prasinophyceae). *Phycologia* 1995;**34**:285–92. https://doi.org/10.2216/i0031-8884-34-4-285.1

Clerissi C, Desdevises Y, Grimsley N. Prasinoviruses of the marine Green alga Ostreococcus tauri are mainly species specific. *J Virol* 2012;**86**:4611–9. https://doi.org/10.1128/JVI.07221-11

Clerissi C, Grimsley N, Ogata H *et al.* Unveiling of the diversity of Prasinoviruses (Phycodnaviridae) in marine samples by using high-throughput sequencing analyses of PCR-amplified DNA polymerase and major capsid protein genes. *Appl Environ Microbiol* 2014;**80**:3150–60. https://doi.org/10.1128/AEM.00123-14

Comeau AM, Bertrand C, Letarov A *et al.* Modular architecture of the T4 phage superfamily: A conserved core genome and a plastic periphery. *Virology* 2007;**362**:384–96. https://doi.org/10.1016/j.virol.2006.12.031

Cottrell M, Suttle C. Wide-spread occurrence and clonal variation in viruses which cause lysis of a cosmopolitan, eukaryotic marine phytoplankter Micromonas pusilla. *Mar Ecol Prog Ser* 1991;**78**:1–9. https://doi.org/10.3354/meps078001

Cottrell MT, Suttle CA. Genetic diversity of algal viruses which lyse the photosynthetic Picoflagellate Micromonas pusilla (Prasinophyceae). *Appl Environ Microbiol* 1995;**61**:3088–91. https://doi.org/10.1128/AEM.61.8.3088-3091.1995

Darling ACE, Mau B, Blattner FR *et al.* Mauve: Multiple alignment of conserved genomic sequence with rearrangements. *Genome Res* 2004;**14**:1394–403. https://doi.org/10.1101/gr.2289704

Dennehy JJ. What can Phages tell us about host-pathogen coevolution? *Int J Evol Biol* 2012;**2012**:396165. https://doi.org/10.1155/2012/396165

Derelle E, Ferraz C, Escande M-L *et al.* Life-cycle and genome of OtV5, a large DNA virus of the pelagic marine unicellular Green alga Ostreococcus tauri. *PLoS One* 2008;**3**:e2250. https://doi.org/10.1371/journal.pone.0002250

Derelle E, Monier A, Cooke R *et al.* Diversity of viruses infecting the Green microalga Ostreococcus lucimarinus. *J Virol* 2015;**89**:5812–21. https://doi.org/10.1128/JVI.00246-15

Derelle E, Yau S, Moreau H *et al.* Prasinovirus attack of Ostreococcus is furtive by day but savage by night. *J Virol* 2018;**92**. https://doi.org/10.1128/JVI.01703-17

Duncan GA, Dunigan DD, Van Etten JL. Diversity of tRNA clusters in the Chloroviruses. *Viruses* 2020;**12**:1173. https://doi.org/10.3390/v12101173

Edwards KF, Hayward C. The dimensionality of infection networks among viruses infecting microbial eukaryotes and bacteria. *Ecol Lett* 2024;**27**:e14383. https://doi.org/10.1111/ele.14383

Emms DM, Kelly S. OrthoFinder: Phylogenetic orthology inference for comparative genomics. *Genome Biol* 2019;**20**:238. https://doi.org/10.1186/s13059-019-1832-y

Endo H, Blanc-Mathieu R, Li Y *et al.* Biogeography of marine giant viruses reveals their interplay with eukaryotes and ecological functions. *Nat Ecol Evol* 2020;1–11. https://doi.org/10.1038/s41559-020-01288-w

Farzad R, Ha AD, Aylward FO. Diversity and genomics of giant viruses in the North Pacific subtropical gyre. *Front Microbiol* 2022;**13**.

Ferris MT, Joyce P, Burch CL. High frequency of mutations that expand the host range of an RNA virus. *Genetics* 2007;**176**:1013–22. https://doi.org/10.1534/genetics.106.064634

Flores, C. O., Meyer, J. R., Valverde, S., Farr, L., & Weitz, J. S. 'Statistical structure of host–phage interactions,' In: *Proceedings of the National Academy of Sciences*, **108**, E288–97, 2011. https://doi.org/10.1073/pnas.1101595108

Fokine A, Rossmann MG. Molecular architecture of tailed double-stranded DNA phages. *Bacteriophage* 2014;**4**:e28281. https://doi.org/10.4161/bact.28281

Fortuna MA, Stouffer DB, Olesen JM *et al.* Nestedness versus modularity in ecological networks: Two sides of the same coin? *J Anim Ecol* 2010;**79**:811–7. https://doi.org/10.1111/j.1365-2656.2010.01688.x

Frada M, Probert I, Allen MJ *et al.* The "Cheshire cat" escape strategy of the coccolithophore Emiliania huxleyi in response to viral infection. *Proc Natl Acad Sci* 2008;**105**:15944–9. https://doi.org/10.1073/pnas.0807707105

Frada MJ, Rosenwasser S, Ben-Dor S *et al.* Morphological switch to a resistant subpopulation in response to viral infection in the bloom-forming coccolithophore Emiliania huxleyi. *PLoS Pathog* 2017;**13**:e1006775. https://doi.org/10.1371/journal.ppat.1006775

Frickel J, Sieber M, Becks L. Eco-evolutionary dynamics in a coevolving host–virus system. *Ecol Lett* 2016;**19**:450–9. https://doi.org/10.1111/ele.12580

Frickel J, Feulner PGD, Karakoc E *et al.* Population size changes and selection drive patterns of parallel evolution in a host–virus system. *Nat Commun* 2018;**9**:1–10. https://doi.org/10.1038/s41467-018-03990-7

Friman V-P, Buckling A. Effects of predation on real-time host–parasite coevolutionary dynamics. *Ecol Lett* 2013;**16**:39–46. https://doi.org/10.1111/ele.12010

Fuhrman JA. Marine viruses and their biogeochemical and ecological effects. *Nature* 1999;**399**:541–8. https://doi.org/10.1038/21119

Fuhrman JA, Campbell L. Microbial microdiversity. *Nature* 1998;**393**:410–1. https://doi.org/10.1038/30839

Gonzalez-Serrano R, Rosselli R, Roda-Garcia JJ *et al.* Distantly related Alteromonas bacteriophages share tail fibers exhibiting properties of transient chaperone caps. *Nat Commun* 2023;**14**:6517. https://doi.org/10.1038/s41467-023-42114-8

Graves MV, Bernadt CT, Cerny R *et al.* Molecular and genetic evidence for a virus-encoded glycosyltransferase involved in protein glycosylation. *Virology* 2001;**285**:332–45. https://doi.org/10.1006/viro.2001.0937

Downloaded from https://academic.oup.com/ve/article/12/1/veaf096/8472608 by guest on 18 February 2026

Guidi L, Chaffron S, Bittner L *et al.* Plankton networks driving carbon export in the oligotrophic ocean. *Nature* 2016;**532**:465–70. https://doi.org/10.1038/nature16942

Guindon S, Dufayard J-F, Lefort V *et al.* New algorithms and methods to estimate maximum-likelihood phylogenies: Assessing the performance of PhyML 3.0. *Syst Biol* 2010;**59**:307–21. https://doi.org/10.1093/sysbio/syq010

Gurevich A, Saveliev V, Vyahhi N *et al.* QUAST: Quality assessment tool for genome assemblies. *Bioinf (Oxf)* 2013;**29**:1072–5. https://doi.org/10.1093/bioinformatics/btt086

Ha AD, Moniruzzaman M, Aylward FO. Assessing the biogeography of marine giant viruses in four oceanic transects. *ISME Commun* 2023;**3**:43. https://doi.org/10.1038/s43705-023-00252-6

Hashemolhosseini S, Holmes Z, Mutschler B *et al.* Alterations of receptor specificities of Coliphages of the T2 family. *J Mol Biol* 1994;**240**:105–10. https://doi.org/10.1006/jmbi.1994.1424

Hingamp P, Grimsley N, Acinas SG *et al.* Exploring nucleocytoplasmic large DNA viruses in Tara oceans microbial metagenomes. *ISME J* 2013;**7**:1678–95. https://doi.org/10.1038/ismej.2013.59

Hoang DT, Chernomor O, von Haeseler A *et al.* UFBoot2: Improving the ultrafast bootstrap approximation. *Mol Biol Evol* 2018;**35**:518–22. https://doi.org/10.1093/molbev/msx281

Holtzman T, Globus R, Molshanski-Mor S *et al.* A continuous evolution system for contracting the host range of bacteriophage T7. *Sci Rep* 2020;**10**:307. https://doi.org/10.1038/s41598-019-57221-0

Huerta-Cepas J, Forslund K, Coelho LP *et al.* Fast genome-wide functional annotation through Orthology assignment by eggNOG-mapper. *Mol Biol Evol* 2017;**34**:2115–22. https://doi.org/10.1093/molbev/msx148

Jain C, Rodriguez-R LM, Phillippy AM *et al.* High throughput ANI analysis of 90K prokaryotic genomes reveals clear species boundaries. *Nat Commun* 2018;**9**:5114. https://doi.org/10.1038/s41467-018-07641-9

Kalyaanamoorthy S, Minh BQ, Wong TKF *et al.* ModelFinder: Fast model selection for accurate phylogenetic estimates. *Nat Methods* 2017;**14**:587–9. https://doi.org/10.1038/nmeth.4285

Kans J. *Entrez Direct: E-Utilities on the Unix Command Line. Entrez Programming Utilities Help [Internet]*. National Center for Biotechnology Information (US), 2021.

Katoh K, Misawa K, Kuma K *et al.* MAFFT: A novel method for rapid multiple sequence alignment based on fast Fourier transform. *Nucleic Acids Res* 2002;**30**:3059–66.

van Kempen M, Kim SS, Tumescheit C *et al.* Fast and accurate protein structure search with Foldseek. *Nat Biotechnol* 2024;**42**:243–6. https://doi.org/10.1038/s41587-023-01773-0

Kizziah JL, Manning KA, Dearborn AD *et al.* Structure of the host cell recognition and penetration machinery of a Staphylococcus aureus bacteriophage. *PLoS Pathog* 2020;**16**:e1008314. https://doi.org/10.1371/journal.ppat.1008314

Krueger F. *TrimGalore!: A Wrapper Tool around Cutadapt and FastQC. Babraham Bioinformatics, Babraham Institute, Cambridge, UK*. 2012.

Labrie SJ, Samson JE, Moineau S. Bacteriophage resistance mechanisms. *Nat Rev Microbiol* 2010;**8**:317–27. https://doi.org/10.1038/nrmicro2315

Lammens K, Bemeleit DJ, Möckel C *et al.* The Mre11:Rad50 structure shows an ATP-dependent molecular clamp in DNA double-strand break repair. *Cell* 2011;**145/1**:54–66. https://doi.org/10.1016/j.cell.2011.02.038

de Leeuw M, Baron M, Ben David O *et al.* Molecular insights into bacteriophage evolution toward its host. *Viruses* 2020;**12**:1132. https://doi.org/10.3390/v1210113

Lemoine F, Gascuel O. Gotree/Goalign: Toolkit and go API to facilitate the development of phylogenetic workflows. *NAR Genom Bioinform* 2021;**3**. https://doi.org/10.1093/nargab/lqab075

Letunic I, Bork P. Interactive tree of life (iTOL): An online tool for phylogenetic tree display and annotation. *Bioinformatics* 2007;**23**:127–8. https://doi.org/10.1093/bioinformatics/btl529

Li H. *Seqtk: Toolkit for Processing Sequences in FASTA/Q Formats*. GitHub; 2012.

Li H, Durbin R. Fast and accurate short read alignment with burrows-wheeler transform. *Bioinf (Oxf)* 2009;**25**:1754–60. https://doi.org/10.1093/bioinformatics/btp324

Listmann L, Peters C, Rahlff J *et al.* Seasonality and strain specificity drive rapid Co-evolution in an Ostreococcus-virus system from the western Baltic Sea. *Microb Ecol* 2023;**86**:2414–23. https://doi.org/10.1007/s00248-023-02243-5

Marston, M. F., Pierciey, F. J., Shepard, A., Gearin, G., Qi, J., Yandava, C., Schuster, S. C., *et al.* 'Rapid diversification of coevolving marine Synechococcus and a virus,' In: *Proceedings of the National Academy of Sciences*, **109**, pp. 4544–9, 2012. https://doi.org/10.1073/pnas.1120310109

Martiny JBH, Riemann L, Marston MF *et al.* Antagonistic coevolution of marine planktonic viruses and their hosts. *Annu Rev Mar Sci* 2014;**6**:393–414. https://doi.org/10.1146/annurev-marine-010213-135108

Mayers KMJ, Kuhlisch C, Basso JTR *et al.* Grazing on marine viruses and its biogeochemical implications. *MBio* 2023;**14**:e01921–1. https://doi.org/10.1128/mbio.01921-21

Michely S, Toulza E, Subirana L *et al.* Evolution of codon usage in the smallest photosynthetic eukaryotes and their Giant viruses. *Genome Biol Evol* 2013;**5**:848–59. https://doi.org/10.1093/gbe/evt053

Middelboe M, Brussaard CPD. Marine viruses: Key players in marine ecosystems. *Viruses* 2017;**9**:302. https://doi.org/10.3390/v9100302

Minh BQ, Schmidt HA, Chernomor O *et al.* IQ-TREE 2: New models and efficient methods for phylogenetic inference in the genomic era. *Mol Biol Evol* 2020;**37**:1530–4. https://doi.org/10.1093/molbev/msaa015

Moore LR, Rocap G, Chisholm SW. Physiology and molecular phylogeny of coexisting Prochlorococcus ecotypes. *Nature* 1998;**393**:464–7. https://doi.org/10.1038/30965

Moreau H, Piganeau G, Desdevises Y *et al.* Marine Prasinovirus genomes show low evolutionary divergence and Acquisition of Protein Metabolism Genes by horizontal gene transfer. *J Virol* 2010;**84**:12555–63. https://doi.org/10.1128/JVI.01123-10

Nandhagopal N, Simpson AA, Gurnon JR *et al.* The structure and evolution of the major capsid protein of a large, lipid-containing DNA virus. *Proc Natl Acad Sci USA* 2002;**99**:14758–63. https://doi.org/10.1073/pnas.232580699

Pandey S, Kirti A, Kumar A *et al.* The SbcC and SbcD homologs of the cyanobacterium anabaena sp. strain PCC7120 (Alr3988 and All4463) contribute independently to DNA repair. *Funct Integr Genomics* 2018;**18**:357–67. https://doi.org/10.1007/s10142-018-0599-7

Papadopoulos V, Baraldi M, Guilarte TR *et al.* Translocator protein (18 kDa): New nomenclature for the peripheral-type benzodiazepine receptor based on its structure and molecular function. *Trends Pharmacol Sci* 2006;**27/8**:402–9. https://doi.org/10.1016/j.tips.2006.06.005

Paterson S, Vogwill T, Buckling A *et al.* Antagonistic coevolution accelerates molecular evolution. *Nature* 2010;**464**:275–8. https://doi.org/10.1038/nature08798

Downloaded from https://academic.oup.com/ve/article/12/1/veaf096/8472608 by guest on 18 February 2026

Pelusi A, De Luca P, Manfellotto F *et al.* Virus-induced spore formation as a defense mechanism in marine diatoms. *New Phytol* 2021;**229**: 2251–9. https://doi.org/10.1111/nph.16951

Retel C, Märkle H, Becks L *et al.* Ecological and evolutionary processes shaping viral genetic diversity. *Viruses* 2019;**11**:220. https://doi.org/10.3390/v11030220

Rey Redondo E, Leung SKK, Yung CCM. Genomic and biogeographic characterisation of the novel prasinovirus Mantoniella tinhauana virus 1. *Environ Microbiol Rep* 2024;**16**:e70020. https://doi.org/10.1111/1758-2229.70020

Schleyer G, Kuhlisch C, Ziv C *et al.* Lipid biomarkers for algal resistance to viral infection in the ocean. *Proc Natl Acad Sci* 2023;**120**:e2217121120. https://doi.org/10.1073/pnas.2217121120

Seemann T. Prokka: Rapid prokaryotic genome annotation. *Bioinformatics* 2014;**30**:2068–9. https://doi.org/10.1093/bioinformatics/btu153

Shao Q, Agarkova IV, Noel EA *et al.* Near-atomic, non-icosahedrally averaged structure of giant virus Paramecium bursaria chlorella virus 1. *Nat Commun* 2022;**13**:6476. https://doi.org/10.1038/s41467-022-34218-4

Short SM, Short CM. Diversity of algal viruses in various north American freshwater environments. *Aquat Microb Ecol* 2008;**51**: 13–21. https://doi.org/10.3354/ame01183

Sirihongthong, T., & Auewarakul, P. Viral codon usage and the virus-host interactions. *Front. Microbiol* 2025:**16**. https://doi.org/10.3389/fmicb.2025.1711603

Speciale I, Notaro A, Abergel C *et al.* The astounding world of Glycans from Giant viruses. *Chem Rev* 2022;**122**:15717–66. https://doi.org/10.1021/acs.chemrev.2c00118

Stern A, Sorek R. The phage-host arms-race: Shaping the evolution of microbes. *Bioessays* 2011;**33**:43–51. https://doi.org/10.1002/bies.201000071

Storvik KAM, Foster PL. The SMC-like protein complex SbcCD enhances DNA polymerase IV-dependent spontaneous mutation in Escherichia coli. *J Bacteriol* 2011;**193/3**:660–9. https://doi.org/10.1128/jb.01166-10

Sullivan MJ, Petty NK, Beatson SA. Easyfig: A genome comparison visualizer. *Bioinformatics* 2011;**27**:1009–10. https://doi.org/10.1093/bioinformatics/btr039

Suttle CA. Viruses in the sea. *Nature* 2005;**437**:356–61. https://doi.org/10.1038/nature04160

Suttle CA. Marine viruses—Major players in the global ecosystem. *Nat Rev Microbiol* 2007;**5**:801–12. https://doi.org/10.1038/nrmicro1750

Tétart F, Repoila F, Monod C *et al.* Bacteriophage T4 host range is expanded by duplications of a small domain of the tail Fiber Adhesin. *J Mol Biol* 1996;**258**:726–31. https://doi.org/10.1006/jmbi.1996.0281

Thingstad TF. Elements of a theory for the mechanisms controlling abundance, diversity, and biogeochemical role of lytic bacterial viruses in aquatic systems. *Limnol Oceanogr* 2000;**45**: 1320–8. https://doi.org/10.4319/lo.2000.45.6.1320

Thomas R, Grimsley N, Escande M *et al.* Acquisition and maintenance of resistance to viruses in eukaryotic phytoplankton populations. *Environ Microbiol* 2011;**13**:1412–20. https://doi.org/10.1111/j.1462-2920.2011.02441.x

Thomas R, Jacquet S, Grimsley N *et al.* Strategies and mechanisms of resistance to viruses in photosynthetic aquatic microorganisms. *Adv Oceanogr Limnol* 2012;**3**:1–15. https://doi.org/10.1080/19475721.2012.672338

Thomy J, Sanchez F, Prioux C *et al.* Unveiling Prasinovirus diversity and host specificity through targeted enrichment in the South China Sea. *ISME Commun* 2024;**4/1**:ycae109. https://doi.org/10.1093/ismeco/ycae109

Tragin M, Vaulot D. Green microalgae in marine coastal waters: The ocean sampling day (OSD) dataset. *Sci Rep* 2018;**8**:14020. https://doi.org/10.1038/s41598-018-32338-w

Tragin M, Vaulot D. Novel diversity within marine Mamiellophyceae (Chlorophyta) unveiled by metabarcoding. *Sci Rep* 2019;**9**:5190. https://doi.org/10.1038/s41598-019-41680-6

Van Etten JL, Gurnon JR, Yanai-Balser GM *et al.* Chlorella viruses encode most, if not all, of the machinery to glycosylate their glycoproteins independent of the endoplasmic reticulum and Golgi. *Biochim Biophys Acta* 2010;**1800**:152–9. https://doi.org/10.1016/j.bbagen.2009.07.024

Van Valen L. Molecular evolution as predicted by natural selection. *J Mol Evol* 1974;**3**:89–101. https://doi.org/10.1007/BF01796554

Wang IN, Li Y, Que Q *et al.* Evidence for virus-encoded glycosylation specificity. *Proc Natl Acad Sci USA* 1993;**90**:3840–4. https://doi.org/10.1073/pnas.90.9.3840

Wang D, Zhang Y, Zhang Z *et al.* KaKs_Calculator 2.0: A toolkit incorporating gamma-series methods and sliding window strategies. *Genomics Proteomics Bioinformatics* 2010;**8**:77–80. https://doi.org/10.1016/S1672-0229(10)60008-3

Waterbury JB, Valois FW. Resistance to co-occurring phages enables marine synechococcus communities to coexist with cyanophages abundant in seawater. *Appl Environ Microbiol* 1993;**59**:3393–9. https://doi.org/10.1128/aem.59.10.3393-3399.1993

Weinbauer MG. Ecology of prokaryotic viruses. *FEMS Microbiol Rev* 2004;**28**:127–81. https://doi.org/10.1016/j.femsre.2003.08.001

Weitz JS, Poisot T, Meyer JR *et al.* Phage–bacteria infection networks. *Trends Microbiol* 2013;**21**:82–91. https://doi.org/10.1016/j.tim.2012.11.003

Weynberg KD, Allen MJ, Gilg IC *et al.* Genome sequence of Ostreococcus tauri virus OtV-2 throws light on the role of Picoeukaryote niche separation in the ocean▽. *J Virol* 2011;**85**:4520–9. https://doi.org/10.1128/JVI.02131-10

Wilhelm SW, Suttle CA. Viruses and nutrient cycles in the sea: Viruses play critical roles in the structure and function of aquatic food webs. *Bioscience* 1999;**49**:781–8. https://doi.org/10.2307/1313569

Winnepenninckx, B., Backeljau, T., & De Wachter, R. Extraction of high molecular weight DNA from molluscs. *Trends Genet* 1993;**9**:407. https://doi.org/10.1016/0168-9525(93)90102-n

Xiang Y, Baxa U, Zhang Y *et al.* Crystal structure of a virus-encoded putative glycosyltransferase. *J Virol* 2010;**84**:12265–73. https://doi.org/10.1128/JVI.01303-10

Yau S, Hemon C, Derelle E *et al.* A viral immunity chromosome in the marine Picoeukaryote, Ostreococcus tauri. *PLoS Pathog* 2016;**12**:e1005965. https://doi.org/10.1371/journal.ppat.1005965

Yau S, Caravello G, Fonvieille N *et al.* Rapidity of genomic adaptations to Prasinovirus infection in a marine microalga. *Viruses* 2018;**10**:441. https://doi.org/10.3390/v10080441

Yau S, Krasovec M, Benites LF *et al.* Virus-host coexistence in phytoplankton through the genomic lens. *Sci Adv* 2020;**6**:eaay2587. https://doi.org/10.1126/sciadv.aay2587

Zborowsky S, Lindell D. Resistance in marine cyanobacteria differs against specialist and generalist cyanophages. *Proc Natl Acad Sci USA* 2019;**116**:16899–908. https://doi.org/10.1073/pnas.1906897116

Zborowsky S, Tahan R, Lindell D. Adaptive loss of tRNA gene expression leads to phage resistance in a marine *Synechococcus* cyanobacterium. *Nat Microbiol* 2025;**10**:66–76. https://doi.org/10.1038/s41564-024-01877-6

Zhao L, Seth-Pasricha M, Stemate D *et al.* Existing host range mutations constrain further emergence of RNA viruses. *J Virol* 2019;**93**:e01385–18. https://doi.org/10.1128/JVI.01385-18

Downloaded from https://academic.oup.com/ve/article/12/1/veaf096/8472608 by guest on 18 February 2026

Zingone A, Sarno D, Forlani G. Seasonal dynamics in the abundance of Micromonas pusilla (Prasinophyceae) and its viruses in the Gulf of Naples (Mediterranean Sea). *J Plankton Res* 1999;**21**: 2143–59. https://doi.org/10.1093/plankt/21.11.2143

Zingone A, Natale F, Biffali E *et al.* Diversity in morphology, infectivity, molecular characteristics and induced host resistance between two viruses infecting *Micromonas pusilla*. *Aquat Microb Ecol* 2006;**41**: 1–14. https://doi.org/10.3354/AME045001

Downloaded from https://academic.oup.com/ve/article/12/1/veaf096/8472608 by guest on 18 February 2026

© The Author(s) 2026. Published by Oxford University Press. This is an Open Access article distributed under the terms of the Creative Commons Attribution License (https://creativecommons.org/licenses/by/4.0/), which permits unrestricted reuse, distribution, and reproduction in any medium, provided the original work is properly cited.
Virus Evolution, 2026, **12**, 1–20
https://doi.org/10.1093/ve/veaf096
Research Article